International Journal of Pharmaceutics 647 (2023) 123535

Contents lists available at ScienceDirect

International Journal of Pharmaceutics

journal homepage: www.elsevier.com/locate/ijpharm

Development and characterization of a poloxamer hydrogel composed of human mesenchymal stromal cells (hMSCs) for reepithelization of skin injuries

Cristina Galocha-León [a], Cristina Antich [b,c,d,e], Ana Voltes-Martínez [b,c,d,e,f], Juan A. Marchal [b,c,d,e,f], Mireia Mallandrich [g,h], Lyda Halbaut [g,h], María J. Rodríguez-Lagunas [i,j], Eliana B. Souto [k,l,*], Beatriz Clares-Naveros [a,c,h,*], Patricia Gálvez-Martín [a,m]

[a] Department of Pharmacy and Pharmaceutical Technology, Faculty of Pharmacy, University of Granada, 18071 Granada, Spain
[b] Biopathology and Regenerative Medicine Institute (IBIMER), Centre for Biomedical Research, University of Granada, 18100 Granada, Spain
[c] Biosanitary Institute of Granada (ibs.GRANADA), University Hospital of Granada-University of Granada, 18100 Granada, Spain
[d] Department of Human Anatomy and Embryology, Faculty of Medicine, University of Granada, 18012 Granada, Spain
[e] Excellence Research Unit "Modeling Nature" (MNat), University of Granada, 18016 Granada, Spain
[f] BioFab i3D Lab - Biofabrication and 3D (Bio)printing Singular Laboratory, University of Granada, 18100 Granada, Spain
[g] Department of Pharmacy and Pharmaceutical Technology and Physical Chemistry, Faculty of Pharmacy and Food Sciences, University of Barcelona, 08028 Barcelona, Spain
[h] Institut de Nanociència i Nanotecnologia IN2UB, Universitat de Barcelona, 08028 Barcelona, Spain
[i] Department of Biochemistry & Physiology, Faculty of Pharmacy & Food Sciences, University of Barcelona, 08028 Barcelona, Spain
[j] Institute of Biomedicine, University of Barcelona, 08028 Barcelona, Spain
[k] UCIBIO – Applied Molecular Biosciences Unit, MEDTECH, Laboratory of Pharmaceutical Technology, Department of Drug Sciences, Faculty of Pharmacy, University of Porto, 4050-313 Porto, Portugal
[l] Associate Laboratory i4HB - Institute for Health and Bioeconomy, Faculty of Pharmacy, University of Porto, 4050-313 Porto, Portugal
[m] R&D Human and Animal Health, Bioibérica S.A.U., 08029 Barcelona, Spain

ARTICLE INFO

Keywords:
Hydrogel
Poloxamer
Human mesenchymal stromal cells
Reepithelization
Wound healing
Pig skin

ABSTRACT

Wound healing is a natural physiological reaction to tissue injury. Hydrogels show attractive advantages in wound healing not only due to their biodegradability, biocompatibility and permeability but also because provide an excellent environment for cell migration and proliferation. The main objective of the present study was the design and characterization of a hydrogel loaded with human mesenchymal stromal cells (hMSCs) for use in would healing of superficial skin injures. Poloxamer 407® was used as biocompatible biomaterial to embed hMSCs. The developed hydrogel containing 20 % (w/w) of polymer resulted in the best formulation with respect to physical, mechanical, morphological and biological properties. Its high swelling capacity confirmed the hydrogel's capacity to absorb wounds' exudate. LIVE/DEAD® assay confirm that hMSCs remained viable for at least 48 h when loaded into the hydrogels. Adding increasing concentrations of hMSCs-loaded hydrogel to the epithelium did not affect keratinocytes' viability and healing capacity and all wound area was closed in less than one day. Our study opens opportunities to exploit poloxamer hydrogels as cell carriers for the treatment of skin superficial wound.

1. Introduction

The skin is the largest organ in the human body, which protects us from microbial infection and external environmental damage. It is made up of three layers, the epidermis (the outer surface of the skin), the dermis (the inner layer of the skin) and the hypodermis, also known as the subcutaneous tissue. The epidermis is populated by keratinocytes, melanocytes, and Merkel cells. On the other hand, the dermis and hypodermis consist of collagen, elastic fibers, glycosaminoglycans, fibroblast and other cells of the immune system (Stan et al., 2021). The skin is

* Corresponding authors at: Laboratory of Pharmaceutical Technology, Faculty of Pharmacy of University of Porto, Porto, Portugal (E.B.S.); and Department of Pharmacy and Pharmaceutical Technology, Faculty of Pharmacy, University of Granada, University Campus of Cartuja, 18071 Granada, Spain (B.C.-N.).
E-mail addresses: ebsouto@ff.up.pt (E.B. Souto), beatrizclares@ugr.es (B. Clares-Naveros).

https://doi.org/10.1016/j.ijpharm.2023.123535
Received 24 August 2023; Received in revised form 14 October 2023; Accepted 17 October 2023
Available online 19 October 2023

often damaged by traumas, severe burns, ulcers and various other injuries, disrupting its protective barrier functions and vital role in sensory perception. After the skin is damaged, the human body reacts to it and immediately initiates the healing process, consisting mainly of haemostasis, inflammation, proliferation and remodelling (de Almeida et al., 2022; de Castro et al., 2023; do Nascimento et al., 2023). In order for a wound to heal properly, the stages should take place in the correct order. In the homeostasis stage, the arteries in the trauma area constrict to reduce blood loss immediately and platelets are then released along with fibrin to form a thrombus or clot to seal the damaged arteries and help prevent bleeding (de Almeida et al., 2022; do Nascimento et al., 2023; Han and Ceilley, 2017). During the inflammatory response, the vascular permeability increases and the inflammatory cells, such as monocytes, lymphocytes and neutrophils are activated, which migrate to the wound in response to chemokines. For the removal of necrotic tissue and foreign bodies as well as initiation and regulation of wound repair, the inflammatory mediators and inflammatory cells are essential (Huang et al., 2022). In the proliferation stage, granulated tissue with an extracellular matrix (ECM) composed of new connective tissue and blood vessels is formed (Liang et al., 2021). Keratinocytes, fibroblasts and vascular endothelial cells through their proliferation and migration activity accomplish wound epithelial regeneration, neovascularization and granulation tissue formation (de Almeida et al., 2022; do Nascimento et al., 2023; Huang et al., 2022). Keratinocytes are involved in the inflammatory reaction and can close the injured site through epithelialization (Wiegand et al., 2021). Remodelling is the final phase of wound healing which the granulation tissue formed in wound healing evolves into normal connective tissue (de Almeida et al., 2022; do Nascimento et al., 2023).

Depending on the duration of the healing stages, wounds are generally classified into acute wounds and chronic wounds. Wounds caused by corrosive chemicals, radioactivity, mechanical injury, heat or electrical shock are considered acute wounds and usually heal in a relatively short time. However, chronic wounds do not follow the orderly stages and predictable times that characterise the normal wound healing process and are associated with specific diseases, such as diabetes mellitus (Naskar and Kim, 2020). Skin wounds can also be categorized into three types based on depth: superficial wounds, partial-thickness wounds, and full-thickness wounds (Da et al., 2017).

In recent years, tissue engineering treatments have emerged as potential therapies. Human mesenchymal stromal cells (hMSCs) are widely used in the wound healing and regeneration process for their regenerative capacity and their possible therapeutical effects (Bian et al., 2022; Guillamat-Prats, 2021; Hu et al., 2018). hMSCs are multipotent stromal cells with the ability to differentiate into mesenchymal tissue lineages such as osteoblasts, chondrocytes, myocytes and adipocytes and they are found in most tissues, but mainly in bone marrow and adipose (Gálvez-Martín et al., 2014). The hMSCs have beneficial effects on skin homeostasis and repair of the lesions due to promote cell differentiation, immune-modulation, secretion of growth factors to promote re-epithelialization and neovascularization and cellular infiltration (Bian et al., 2022; Guillamat-Prats, 2021; Rodrigues et al., 2014). The most limiting for the therapeutic efficacy is the poor delivery and viability of the transplanted hMSCs in the desired site of action, such as skin wounds. Thus, hMSCs need to be effectively delivered while remaining in contact with the skin lesion environment (Soriano-Ruiz et al., 2019a).

Hydrogels are an attractive alternative as delivery vehicles of stem cells to the wound site due to ensure the sustained viability and functionality of the stem cells and thus improve their transplantation efficiency (Kaisang et al., 2017; Stan et al., 2021). Hydrogels are hydrophilic gels a with three-dimensional elastic and porous network structures and they have good biodegradability, biocompatibility, adhesion, air permeability, and maintain a moist environment for cell migration and can effectively promote cell proliferation and migration facilitating the process of wound healing. These properties make hydrogels an excellent candidate product for use in skin tissue engineering (Zielinska et al., 2023). Poloxamers, also known by the names of Pluronic®, Synperonic®, and Lutrol® are a family of triblock copolymers with a center block of hydrophobic polypropylene oxide (PPO) which is linked to two hydrophilic polyethylene oxide (PEO) blocks (Fakhari et al., 2017; Giuliano et al., 2020). Poloxamer 407 is known as an "inactive ingredient" by U.S. Food and Drug Administration (FDA) for different types of preparations for use in humans (de Castro et al., 2023; Dumortier et al., 2006; Kaisang et al., 2017). Poloxamer 407 aqueous solutions show thermo-reversible properties. The gelation phenomenon is reversible and is characterised by a sol–gel transition temperature ($T_{sol\text{-}gel}$). Below this temperature, the poloxamer 407 aqueous solutions remains fluid and above this temperature, becoming semi-solid material. The thermo-gelation results to hydrophobic interactions between the poloxamer 407 copolymer chains. By elevating the temperature, the poloxamer 407 copolymer chains aggregate into micellar. The micellization is a result of the dehydration of the hydrophobic PPO blocks (Dumortier et al., 2006; Fakhari et al., 2017). The thermal-sensitivity of the Poloxamer 407 hydrogel allows it to encapsulate cells easily and to favour the attachment of a high number of cells to the site of the defect (Kaisang et al., 2017). Thus, based on all the above mentioned, the main purpose of this study was the design and characterization of a poloxamer-based hydrogel, as well as the evaluation of its suitability for the support of hMSCs aimed for use in would healing of superficial skin injures.

2. Materials and methods

2.1. Materials

Pluronic® F-127 (poloxamer 407®) was purchased from BASF (Ludwigshafen, Germany). Glucose 5 %, Lactated Ringer's solution and Albumin 20 % were purchased from Grifols (Barcelona, Spain). Phosphate-buffered saline (PBS), Dulbecco's modified Eagle's medium (DMEM), collagenase type IA and Fetal Bovine Serum (FBS) were purchased from Sigma-Aldrich Chemie (St Louis, MO, USA). Penicillin–streptomycin antibiotic was purchased from Invitrogen (Merelbeke, Belgium). Trypsin was purchased from Gibco (Invitrogen, Grand Island, NY, USA). Water used in the experiments was obtained from a Milli-Q® System (Merck Millipore Co., Germany). All other chemicals were of analytical grade and used without further purification.

2.2. Preparation of poloxamer-based hydrogels

Four formulations of hydrogels were prepared with different concentrations of Pluronic® F-127: 5, 10, 15 and 20 wt% (named HYP5, HYP10, HYP15 and HYP20 respectively). Firstly, the polymer was sterilized by autoclaving (20 min, 121 °C), and then it was mixed with a sterile packaging medium composed by 50 % of Glucose 5 %, 45 % of Lactated Ringer's solution and 5 % of Albumin 20 % at room temperature. A control formulation was prepared without Pluronic®. Hydrogels were prepared by dispersing the polymer with manual stirring and stored at 4 °C for at least 24 h to ensure complete dissolution to yield clear and homogenous hydrogels.

2.3. Isolation of hMSCs and cell encapsulation

hMSCs were obtained from infrapatellar fat pad of patients with osteoarthritis (OA) during joint replacement surgery. Fat tissue was collected after informed consent from all patients and approval from the Ethics Committee of Clinical University Hospital of Málaga, Spain. To isolate the hMSCs, fat tissue was minced and digested using enzymatic solution of 1 mg/mL collagenase type IA at 37 °C for 1 h on a shaker. After digestion, collagenase was removed by a single wash in sterile PBS, followed by two further washes in DMEM supplemented with 10 % FBS. The cell pellet was resuspended in DMEM containing 20 % FBS, 100 U/

mL penicillin and 100 mg/mL streptomycin and cultured at 37 °C in 5 % CO_2. At 80 % of confluency the cells were released with trypsin and subcultured. Cells were used between passages 3 and 5 for all the experiments. Cells-laden hydrogels (named: HYP5-C, HYP10-C, HYP15-C and HYP20-C) were prepared in three consecutive steps. First, the poloxamer was mixed with 90 % of packaging medium to create the hydrogel as is described in Section 2.1. Second, hMSCs were suspended in the rest of packaging medium (10 %) at a cell density of 1×10^6 cells/mL, after 24 h gelation. Finally, the cellular suspension was incorporated into a vial with the hydrogel at room temperature and under aseptic conditions. Each vial was shortly stirred to obtain a homogeneous distribution of cells and stored at 4 °C over the desired period. The composition of each hydrogel is reported in Table 1.

2.4. Cell culture of keratinocytes

Human primary epidermal keratinocytes (HEKa) were obtained from American Type Culture Collection (ATCC, Manassas, VA, USA) and maintained in EpiLife medium (Gibco Waltham, MA, USA) containing HKGS (Gibco) at 37 °C in a humidified atmosphere containing 5 % CO_2. HEKa cells were seeded on cell culture plates at a density of 10,000 cells/cm^2 and cultured until confluency when the wound-healing assay was performed.

2.5. Biological tissue for ex vivo bioadhesion assays

Pig skin was obtained from pigs in accordance with protocols prescribed by the Animal Experimentation Ethics Committee of the University of Barcelona, Spain (CEEA-UB) code 10617. Female pigs weighing 20–25 kg, were anesthetized with intramuscular administration of ketamine HCl (3 mg/kg), xylazine (2.5 mg/kg) and midazolam (0.17 mg/kg). Propofol (3 mg/kg) was administered via atrial vein after sedation and immediately afterwards they were intubated and maintained under anaesthesia inhaled with isoflurane. Finally, three animals were sacrificed under veterinary supervision at the Animal Facility of the Bellvitge Campus of the University of Barcelona (Spain) using an overdose of sodium thiopental. Pig skin was maintained in HBSS and refrigerated until experiments (Amores et al., 2014). Before use, the pig skin was superficially cleaned with gauze soaked in 0.05 % dodecyl sulphate solution, followed by distilled water.

2.6. Macroscopic analysis of the prepared hydrogel formulations

The physical appearance of the prepared cells-free hydrogels and cells-laden hydrogels was inspected visually after 72 h of preparation in relation to macroscopic aspect and color.

2.7. Cell viability

Viability of hMSCs embedded in the hydrogel formulations was determined by trypan blue dye exclusion staining and posterior cell counting in a Neubauer chamber. It was performed at 0, 24, 48 h after embedding cells into hydrogel at 4 °C and 37 °C. A fluorescence microscope (Olympus IX71; Olympus, Tokyo, Japan) was used to observe the cells. Each sample was counted three times and the average was calculated. The percentage of viability was calculated using the following equation:

$$Cellviability(\%) = \frac{Numberofviablecells}{Totalnumberofcells} \times 100 \quad (1)$$

Table 1
Composition (g) of different cells-loaded hydrogels formulations (final volume: 50 mL).

Formulations	Pluronic®	Packaging Medium	Mesenchymal Stromal Cells
HYP5-C	2.5	47.5	5×10^7
HYP10-C	5	45	5×10^7
HYP15-C	7.5	42.5	5×10^7
HYP20-C	10	40	5×10^7
Control	–	50	5×10^7

2.8. Cell distribution

The hMSCs distribution in each hydrogel was evaluated by Live/Dead kit assay (Invitrogen Inc, USA), following the manufacturer's instruction. It was performed at 0, 24, 48 and 72 h after embedding cells into hydrogel at 4 °C and 37 °C. Briefly, cells-laden hydrogels were stained with 5 μL of 2 μM calcein AM and 10 μL of 4 μM ethidium homodimer-3 in 4 mL of sterile PBS (with calcium), and incubated in the dark for 30 min, to stain dead cells in red and live cells in green. After staining, samples were washed with PBS and observed under a confocal microscope (Zeiss LSM 710). Images were evaluated with the software ImageJ. For each sample, four regions were counted to obtain an average value of percent viable cells.

2.9. hMSCs karyotyping analysis

The hMSCs were analyzed before and after embedding cells into hydrogel. Karyotype analysis was performed by G band techniques (Bayani and Squire, 2004). In order to obtain chromosomal preparations, the hMSCs were treated with 0.8 mg/mL colchicine and incubated at 37 °C for 1.15 h. Briefly, cells were washed with 1 mL trypsin twice. Then, 2 mL trypsin was added at 37 °C for 2 min and centrifuged at 400g for 10 min with 1 mL FBS. The pellet was suspended in 5 mL 75 mM KCl at 37 °C for 20 min and centrifuged at 400 g for 10 min. The cells were fixed with 5 mL methyl alcohol–acetic acid mixture (3:1 v/v) and centrifuged at 400 g for 10 min, this process was repeated twice more. For each karyotype 20 metaphases were analyzed. The result was described to account the recommendations from the International System for Human Cytogenetic Nomenclature (Gonzalez Garcia and Meza-Espinoza, 2006).

2.10. Physicochemical characterization of hydrogels

2.10.1. Gelation time and osmolality

For the determination of gelation time, 5 mL sample was put into a transparent vial with a magnetic bar and placed in a low temperature water bath. The solution was then heated from 10 to 37 °C ± 0.1 °C while being stirred (200 rpm). The gelation time and gelation temperature was measured in triplicate, once the magnetic bar stopped moving due to gelation (Soriano-Ruiz et al., 2020). The gelation process was also studied using the test tube inversion test (Dong et al., 2023). The states of the hydrogels at different temperatures were photographed. Osmolality was determined using a micro-osmometer model 3320 (Advanced Instruments, Inc., Norwood, MA, USA). This instrument measures the freezing point depression (FPD), which is directly proportional to the concentration of osmotically active compounds in aqueous solutions.

2.10.2. Swelling test

The swelling ratio (SR) was assessed by a gravimetric method (El Moussaoui et al., 2021). The swelling properties of hydrogels were determined using lyophilized samples. Lyophilized dry hydrogels samples (0.05 g, n = 3) were incubated in 100 μL PBS at different pH (pH = 7.4 and pH = 5.5) at 37 °C. At selected time intervals the swollen hydrogels were removed and weighed after blotting the excess of PBS with a filter paper. Hydrogels were then replenished with fresh PBS. The swelling ratio was calculated based on the following:

$$SR\,(\%) = \frac{Ws - Wd}{Wd} \times 100 \quad (2)$$

where W_s and W_d are the weight of the swollen and dried hydrogel

samples respectively.

2.10.3. In vitro degradation analysis

The degradation as percentage of weight loss (WL) was calculated by incubating of fresh hydrogels (W_i) (0.5 g) in 1 mL PBS at different pH (pH = 5.5 and pH = 7.4) and at 37 °C. At regular time intervals, hydrogels were dried and weighed (Wt) after blotting the surface PBS. Briefly, the samples were put back in fresh PBS. The degradation was determined in triplicate at each time point and for each pH (El Moussaoui et al., 2021). WL was calculated as follows:

$$WL\,(\%) = \frac{Wi - Wt}{Wi} \times 100 \quad (3)$$

2.10.4. Spreadability test

Spreadability was determined using a manual technique. After 24 h encapsulation, a cylindrical shaped of hydrogel (0.5 g) was obtained using a microtome. Then, the hydrogel was pressed between the surface of microtome and a graduated glass plate (6 × 6 cm, 25 g), on which weights of 20, 50, 100, 200 and 500 g were place at intervals of 1 min. The perpendicular diameters were determined during each interval and the results were expressed as the area (mm^2) (Contreras and Sanchez, 2002). The spreadability of cells-laden hydrogel was determined in triplicate at 25 °C and 37 °C and compared with a free-cells hydrogel.

2.10.5. Rheological analysis

The rheological characterization was conducted using the same equipment, under both oscillation and rotational modes, to evaluate changes induced by the addition of cells. Investigations into the properties of hydrogels were undertaken, with a particular focus on attributes such as viscosity, flow properties, and viscoelasticity. It is critical to understand these rheological properties in the process of designing and selecting hydrogels for specific applications. This ensures that their behavior under different conditions aligns with the intended purpose.

2.10.5.1. Oscillatory studies. The influence of temperature on the rheological properties of the formulations was examined through a temperature sweep ranging from 10 to 40 °C. This operation was conducted using a Haake RheoStress 1 rheometer (Thermo Fischer Scientific, Karlsruhe, Germany) connected to a Thermo Haake Phoenix II + Haake C25P temperature controller. The rheometer was outfitted with a mobile Haake PP60Ti plate (60 mm in diameter), operating in oscillation mode at a constant stress of 0.5 Pa. This value was selected based on a prior stress sweep test, which demonstrated that this stress level fell within the viscoelastic region. The rheometer operated at a standard frequency of 1 Hz, a value selected after a frequency sweep test. Each sample was equilibrated by placing it within the plate-plate sensor system (with a gap of 1 mm) for a duration of 5 min, enabling it to reach the initial temperature of 10 °C. Subsequently, the temperature was incrementally increased from 10 to 40 °C, adhering to a controlled ramp speed sustained over a duration of 2070 s. Throughout this process, measurements were made of the elastic modulus (G'), the viscous modulus (G''), and the complex viscosity (η^*). Determining the crossover of moduli ($G' = G''$) is a commonly employed method for identifying the sol–gel transition point in thermosensitive hydrogels [30,31].

2.10.5.2. Rotational studies. Flow behavior and viscosity determination were carried out with the same rheometer, but equipped with a Haake C60/2Ti mobile cone (60 mm diameter, 0.102 mm gap, and 2° angle) operating in rotation mode. Each sample was equilibrated by placing it between the cone-plate sensor system (0.102 mm gap) for 5 min to attain the running temperature. Viscosity curves and flow curves were recorded for 1 min during the ramp-up period from 1 to 100 s^{-1}, 1 min at 100 s^{-1} (constant shear rate period), and finally during the ramp-down period from 100 to 1 s^{-1}. Data from the flow curve (when they were found to be non-Newtonian) were fitted to different mathematical models, equations (4) – (8) using the Prism®, V. 3.00 software (GraphPad Software Inc., San Diego, CA, USA) in order to determine the flow type:

$$\tau = \tau 0 + \eta p \times \gamma \quad \text{Bingham} \quad (4)$$

$$\tau = k \times (\gamma)^n \quad \text{Ostwald} - \text{De} - \text{Waele} \quad (5)$$

$$\tau = \tau 0 + k1 \times (\gamma)^n \quad \text{Herschel} - \text{Bulkley} \quad (6)$$

$$\sqrt{\tau} = \sqrt{\tau 0} + \sqrt{k1 \times \gamma} \quad \text{Casson} \quad (7)$$

$$\frac{\eta - \eta}{\eta 0 - \eta \infty} = \frac{1}{(1 + (\lambda\gamma)^m)} \quad \text{Cross} \quad (8)$$

The mean viscosity value (Pa•s) was determined from the constant shear section at 100 s^{-1} of the viscosity curve with respect to temperature. The determination of the disturbance of the microstructure during the test evaluated by determining the area of hysteresis loop.

2.10.6. Porosity analysis

The porosity of the hydrogel was calculated according to the Archimede's principle (El Moussaoui et al., 2021). The porosity analysis was carried out by immersion of the lyophilized hydrogels (0.1 g) in 200 mL PBS (pH = 5.5 and pH = 7.4) at room temperature. The submerged mass of the hydrogel was recorded and then the hydrogel was removed, and the wet mass was recorded. Triplicate pH = 5.5 and pH = 7.4 samples were used for the study. Porosity of hydrogels were calculated using the following equation:

$$\text{Porosity}\,(\%) = \frac{Mw - MD}{Mw - MSUB} \times 100 \quad (9)$$

where Mw is the water saturated wet mass of the hydrogel, MD is the dry mass of the hydrogel, and MSUB is the submerged mass of the hydrogel.

2.10.7. Water contact angle measurement

The surface wettability of the hydrogels was determined by calculating the water contact angles in fresh samples at room temperature. Contact angles were determined using Contact Angle Goniometer (Ramé-hart Instrument co, USA). A uniform drop of distilled water (30 μL) was dispensed on the hydrogel surface. The contact angle was evaluated for a precise interval of time from 1 to 10 min until the drop had disappeared. Each measurement was carried out in triplicate and the average value was reported.

2.10.8. Conductivity

Electrical conductivity of the hydrogels was measured with a conductivity meter Crison EC-Meter BASIC 30+ (Crison Instruments, Alella, Spain). The hydrogels were dilute in in PBS 1:20 (pH = 5.5 and pH = 7.4). An electrode of the device was dipped into a glass vial of the samples. Data were expressed as mean ± SD (n = 3).

2.10.9. Determination of the zeta potential

Surface electrical properties of the hydrogels were determined in a Zetasizer Nano ZS (Malvern Instruments Ltd., Malvern, UK), which estimates the zeta potential of samples placed in cells (cuvettes), determining the electrophoretic mobility through Henry equation by measuring the velocity of the particles using Laser Doppler Velocimetry (ZetaSizer, 2023). The zeta potential of the hydrogels was measured at different pH values (pH 4–pH 8), and under a constant 10^{-3} M KNO^3 concentration after suitable dilution (0.1 % w/v) of the hydrogel. Zeta potential determinations were determined after contact during 24 h under mechanical stirring (50 rpm) and at room temperature (Pretel et al., 2017). Values are reported as the mean ± SD of three replicates.

2.10.10. Leakage test

The leakage test was conducted in agar gel surface (Esposito et al., 2016). For this task agar (1.5 %, W/W) was dissolved in simulated PBS 7.4 and PBS 5.5 and stirred at 95 °C until solubilization. Enough quantity was added to form a thin layer in glass slides and kept at room temperature until the gel was obtained. Furthermore, assayed samples were colored with methylene blue to improve observation. About 50 mg of samples were placed onto the end of agar slides, which were put vertically at an angle of 90° and maintained at 4, 25 and 37 ± 0.5 °C. The running distance covered by samples was measured 1, 5 and 10 min after the placement. Leakage value was calculated as the mean ± SD of three replicates.

2.10.11. Evaluation of bioadhesive properties

The ex vivo bioadhesive properties of the formulation are measured by testing its resistance or tension when attempting to break the bond between the tissue epithelial membrane and the formulation. To do this, we developed a simple device for determining the bioadhesive force of the formulation (Li et al., 2012; Mei et al., 2017; Yang et al., 2017). We cut pieces of pig skin to a size of 2.5 × 2.5 cm and fixed them onto two plates, respectively. One plate was fixed onto a stainless-steel base, and the other was connected to a firm thread that fastened a light plastic beaker through a fixed little crown block. We placed 0.3 g of the sample between two pieces of tissue and slightly pressed the upper plank using our hand. We then dropped water into the beaker at a speed of 1.0 mL/min until the two planks were pulled apart due to the gravity of the water on the beaker. The test was carried out at different temperatures, 32 and 37 °C. Finally, we weighed the beaker with water and calculated the bioadhesive force (F, mN/cm^2) using the following equation:

$$F = \frac{W \times g}{A} \tag{10}$$

where W is the mass of water, g is the acceleration due to gravity, and A is the surface area of the applied formulation. The bioadhesive force was presented as mean values ± SD of three replicates. The bioadhesive property of poloxamer 407 formulations was also evaluated measure the influence of the samples on the zeta potential of mucin (Abdellatif et al., 2020; Mendes et al., 2018). Each sample was dispersed with an equivalent amount of 1 % (w/v) of e mucin solution under stirring. The mixtures of hydrogel-mucin were allowed to equilibrate overnight at room temperature. The surface charge of samples was detected using a Zetasizer Nano ZS (Malvern Instruments Ltd., Worcestershire, UK). Readings were reported as the mean ± SD of nine replicates.

2.10.12. Extrudability study

This test measures the required force to remove the hydrogel from the container. The extrudability (E, g/cm^2) of the development hydrogels was evaluated by measurement of the weight necessary to be applied to remove an amount of the hydrogels from 2, 5 and 10 mL syringes. About 2, 5 and 10 g of each formulation were carefully loaded into syringe avoiding the formation of air bubbles. The device was vertically placed on a support and known weight was added to its plunge. The plunger was pressed down and the extruded weight was recorded. The system was maintained at 4 and 25 ± 0.50 °C, to simulate application conditions. The extrudability of developed hydrogels was calculated according to the following equation:

$$E = \frac{W}{A} \tag{11}$$

where W is the weight applied (g) to extrude the gel from de tube and A the area (cm^2) of the extruded hydrogel from the tube. The data obtained were expressed as the mean ± SD of three replicates.

2.10.13. Spray angle

To measure the spray angle, a plastic with a dip tube diameter of 1.2 mm and an aperture size of 0.3 mm was used. The spray was actuated in horizontal direction onto a white paper mounted at a distance of 15 cm from the nozzle. Assayed samples were colored with methylene blue to improve observation. The test was carried out at 4, 10 °C and 25 °C to simulate application conditions. The radius of the circle, formed on the paper, was recorded (Umar et al., 2020). Spray angle is calculated from the following equation:

$$Sprayangle = tan^{-1}x(l/r) \tag{12}$$

where l is a distance of the paper from the nozzle and r is the radius of the circle.

2.10.14. Thermogravimetric analysis (TGA) and differential scanning calorimetry (DSC)

Thermogravimetric analysis (TGA) and differential scanning calorimetry (DSC) were performed with a Mettler Toledo mod. TGA/DSC1 calorimeter (Mettler Toledo, Barcelona, Spain), equipped with a sensor and FRS5 microbalance (precision 0.1 μg). Samples (11–24 mg) have been sealed in aluminium-cells and brought to the initial temperature. The heating rate was 10 °C/min in the 28–950 °C temperature range. Nitrogen was used as purge gas under 50 mL/min flow. The DSC thermogram has also been recorded in the temperature range from −5 to 70 °C. The measures were performed using a METTLER-TOLEDO mod. TGA/DSC1 instrument. Samples (17 mg) were sealed in aluminium-cell and brought to the initial temperature. The heating rate was 2 °C/min, and nitrogen was used as purge gas under 50 mL/min flow.

2.11. Morphological characterization

2.11.1. Size

Mean particle diameter and polydispersity index (PdI) were analyzed by photon correlation spectroscopy (PCS, Zetasizer Nano ZS, Malvern Instruments Ltd., UK) at 4, 32 and 37 °C after suitable dilution of the hydrogel (0.1 %, w/v). Each measurement was carried out in triplicate and the average value was reported.

2.11.2. Environmental scanning electron microscopy analysis

The internal microstructures of hydrogels were analyzed using a scanning electron microscopy (SEM). Sample preparation was performed by freezing in liquid nitrogen and freeze-drying. Then, it was sputter coated with a thin layer of silver. The prepared samples were observed using a Field Emission Scanning Electron Microscope System (FE-SEM; Gemini Carl ZEISS).

Lyophilization induces rapid cooling and phase separation followed by sublimation under vacuum, which alters the porosity of hydrogels and leads to void formation in their structure (Soriano-Ruiz et al., 2019a). Therefore, we also analyzed the samples using the critical point drying technique. HYP20 and HYP20-C hydrogels were fixed with a solution of glutaraldehyde 2.5 % w/v (Merck, Darmstadt, Germany) in 0.1 M sodium cacodylate buffer (Electron Microscopy Sciences, Hatfield, PA, USA), during 2 h at 4 °C, and then washed three times every 15 min with the same buffer solution. Hydrogels were processed using the critical point drying technique. First, they were fixed with 1 % w/v osmium tetroxide for 1 h at room temperature and washed with bidistilled water three times every 5 min. Then, they were dehydrated in a series of ethanol solutions with increasing concentration (50 %, 70 %, 90 %, and 100 %) at 4 °C for 15 min each. The samples were critical point dried in a Leica EM CPD300 dryer (Leica Microsystems, Wetzlar, Germany). Finally, samples were deposited on a double-coated carbon conductive tape, and covered by evaporating them in a high-vacuum thermal evaporator Emitech K975X before being observed in high-vacuum mode.

2.11.3. Lyophilization and relationship with the extrusion process

1.0 mL of each formulation (HYP20 y HYP20-C) was loaded into a syringe at 4 °C and 25 °C. The hydrogels were unloaded into separate

Eppendorf tubes once (1X) with a syringe. The samples were immediately lyophilized, fractured cryogenically, metallized and then analyzed through a microscope. For scanning microscope analysis, samples were mounted on SEM holders using a double carbon tape and also were covered with a gold thin film in order to improve their electrical conductivity (Bio-Rac SC-510). The samples were observed with a Jeol JSM-7001F (Jeol, Japan) operated at 15 kV performed on the TEM-SEM Electron Microscopy Unit from Scientific and Technological Centers (CCiTUB), Universitat de Barcelona.

2.12. Wound-healing assay

The day of the assay the medium was changed and HEKa confluent cultures were scratched with a 200 μL pipette tip in the middle of the well and HYP20-C hydrogel were added at different proportions (30,000, 60,000 and 120,000 hMSCs/well). For better visualizing the HEKa layer, the highest concentration was also tested by separating the hMSCs cells by introducing them into an insert. Before and after 4 h incubation, the width of wounds was photographed with a fluorescent cell imager (Zoe, Bio-Rad, Germany). The wound area was calculated using the Image J public domain software. The percentage of wound area reduction was calculated from the following equation:

$$Woundclosure(\%) = \left(\frac{A0 - At}{A0}\right) \times 100 \quad (13)$$

where A0 is the area of the wound (cell-free area) measured at the initial time, and At is the area of the wound measured 4 h after scratching (Augustine et al., 2018).

2.13. Statistical analysis

Tests for significant differences between means were performed by Student's *t*-test or one-way ANOVA using the Prism®, V. 3.00 software (GraphPad Software Inc., San Diego, CA, USA). Differences where p less than 0.05 were considered statistically significant. Experiments were repeated on three different samples and the results were expressed as mean ± standard deviation (SD).

3. Results

3.1. Effect of Pluronic-127 concentration on hMSCs

To optimize the polymer concentration, the cell viability of cells-laden hydrogels was investigated using hMSCs at a cell density of 1 ×

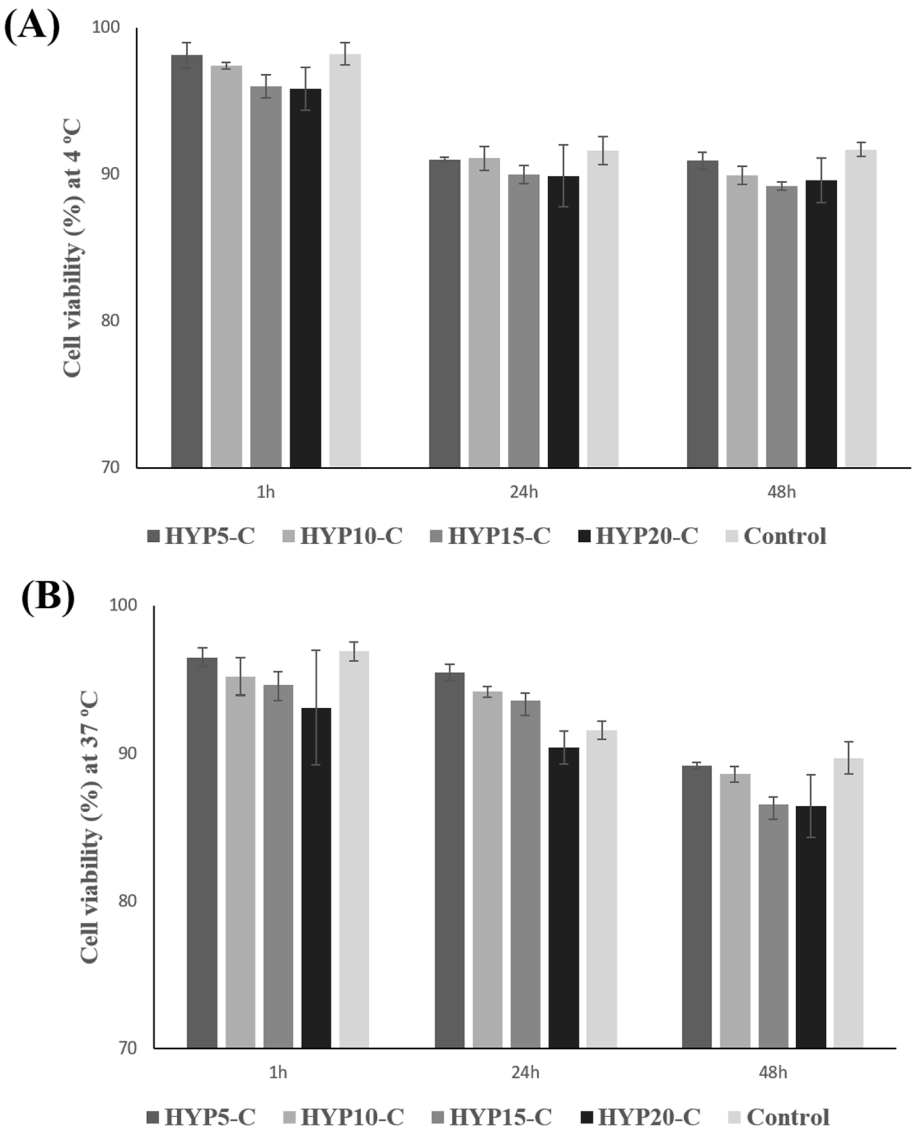

Fig. 1. Cell viability of hMSCs embedded in hydrogels stored at 4 °C, (A) and 37 °C (B) for 3 days. Error bars represent SD (n = 3).

10^6 cells/mL. Cell viability was studied from each hydrogel formulation (control, 5, 10, 15 and 20 % of Pluronic) incubated at 4 °C and 37 °C by trypan blue dye exclusion staining. Generally, there was a high cell survival for all conditions during the evaluated period (Fig. 1). The results showed that the cell viability of Pluronic-based hydrogels at 4 °C for 48 h (90.9 % for HYP5-C, 89.9 % for HYP10-C, 89.6 % for HYP15-C and 89.2 % for HYP20-C), was slightly higher than at 37 °C (89.2 % for HYP5-C, 88.6 % for HYP10-C, 86.5 % for HYP15-C and 85.4 % for HYP20-C). Comparing these results with the cell viability of the control hydrogel at 4 °C and 37 °C (91.7 % and 89.7 % respectively), no significant changes were observed for HYP5-C and HYP10-C hydrogels. However, a slight decrease of their cell viability was observed for HYP15-C and HYP20-C hydrogels. Although significant differences were obtained, all developed formulations kept the cell viability above 85 %, being an acceptable value according to the requirements of the Food and Drug Administration and of the European Medicines Agency for Advanced Therapies Medicinal Products (ATMPs), which define that the cell viability of an ATMP before to be administered must be ≥70–80 % (Guadix et al., 2019). The choice of optimal hydrogel was therefore based on the results obtained in terms of biocompatibility, optical and gelling properties.

All formulated cell-loaded hydrogels showed a homogenous and transparent aspect and white color like the cell-free hydrogels. Therefore, the presence of hMSCs showed significant differences according to the physical appearance of the hydrogels. According the results of macroscopic analysis, cell viability and gelation time of the cells-loaded hydrogels previously studied, HYP5-C, HYP10-C and HYP15-C were excluded from further characterizations and studies. Hence, the HYP20-C hydrogel was more widely investigated.

3.2. Cell distribution

The LIVE/DEAD® assay was employed to visualize the presence and distribution of living and dead cells after 1, 24, 48 and 72 h in the HYP20-C hydrogel at 4 °C and 37 °C (Fig. 2).

Images of confocal microscope revealed a homogeneous distribution of hMSCs within the HYP20-C hydrogel (Fig. 2**B**). These also showed that the hMSCs lost their typical polygonal morphology and maintained their rounded appearance after 72 h (Fig. 2**B**). Results from cell counting indicated that hMSCs in the HYP20-C hydrogel remain viable at 4 °C for 72 h (88 %), as few dead cells were observed. However, at 37 °C the number of dead cells increased, and therefore the cell viability decreased from 95.6 % to 40.7 % after 72 h. (Fig. 2**A**). Thus, 4 °C was found the most suitable temperature for maintaining cells viable for longer time.

3.3. hMSCs karyotyping analysis

Cells were tested for genomic stability using a conventional analysis by G band techniques to check whether the hMSCs maintained their normal karyotype in the cell-load hydrogel (HYP20-C) at 4 °C. The results showed that on passage 3, before embedding cells into hydrogel, the hMSCs were normal diploid karyotype (46, XY). After 48 h

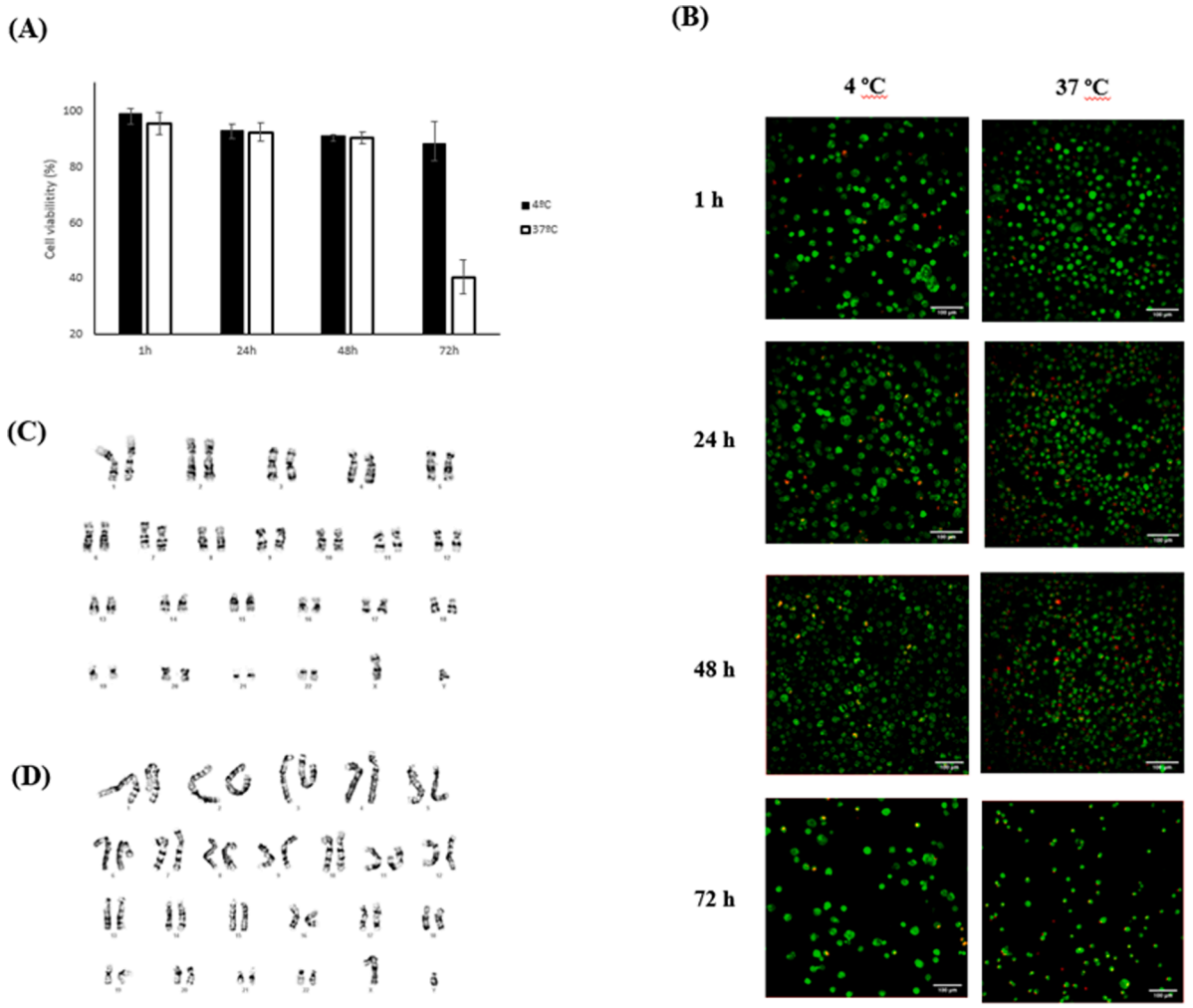

Fig. 2. Live/Dead cell imaging analysis. (A) Percentage of hMSCs viability in HYP20-C hydrogel at 4 °C and 37 °C after 1, 24, 48 and 72 h. (B) Representative image of hMSCs in HYP20-C hydrogel, showing live (green) and dead (red) cells. (C) Karyotype of hMSCs.

formulation at 4 °C, a sample of HYP20-C was studied. The results showed no karyotype changes in the HYP20-C, obtaining a normal diploid karyotype (46, XY) (Fig. 2**C**).

3.4. Physicochemical characterization of hydrogels

3.4.1. Gelation time and osmolality

The gelation temperature and gelation time of HYP20 and HYP20-C formulations were evaluated. Fig. 3 shows the images obtained from the tube inversion test. The gelation temperature of the HYP20 formulation was 24.6 ± 0.5 °C and was reached after 105.6 ± 3.2 s. However, the HYP20-C formulation gelled at a temperature of 23.8 ± 0.3 °C and the gelation time was 102.7 ± 2.5 s.

Osmolality values of HYP20 and HYP20-C formulations were 732 ± 16.64 MOsm/Kg and 361.3 ± 3.21 MOsm/Kg, respectively. These results showed that the addition of the cells reduced the osmolality value of the formulation.

3.4.2. Swelling and degradation properties of HYP20 hydrogels

The ability to absorb liquid and of swelling is an important factor in the development of hydrogels. In wound healing, this property could help to adsorb exudates and provide mechanical resistance to the delivery system at the biological site of action (Ho et al., 2022; Nurzynska et al., 2021; Qing et al., 2021; Zielińska et al., 2022). The swelling properties of HYP20 and HYP20-C hydrogels were evaluated based on their ability to a liquid absorption. The samples of lyophilized hydrogels were immersed in PBS (pH = 7.4 and pH = 5.5) at 37 °C for up to 30 min. Fig. 4**A** shows the swelling behavior of HYP20 and HYP20-C hydrogels at two different pH values. It can be observed higher swelling rate at pH = 5.5 reaching values of 221 ± 6.59 % for HYP20 hydrogel and 297 ± 2.09 % for HYP20-C hydrogel. At pH = 7.4, similar swelling values were obtained for both hydrogels, 223 ± 41.86 % for the HYP20 hydrogel and 218 ± 27.47 % for the HYP20-C hydrogel. HYP20-C hydrogel at pH = 5.5 was the formulation with the best swelling pattern, i.e., the highest swelling ability. On the other hand, it can be observed how all hydrogels decreased their weight after 15 min due to the degradation of the hydrogel.

The degradation of HYP20 and HYP20-C hydrogels was evaluated as percentage of weight loss. It was evaluated in terms of the change of the dry weight of the hydrogels after to be immersed in PBS (pH = 7.4 and pH = 5.5) at 37 °C for 120 min (Fig. 4**B**). The results showed that HYP20 and HYP20-C hydrogels at pH = 5.5 (94.5 ± 0.92 %, 95.25 ± 0.46 %) and at pH 7.4 (92.07 ± 0.48 %, 92.18 ± 2.62 % respectively) were degraded after 120 min. During the first 60 min, the degradation of HYP20 hydrogel was slower to both pH (7.4 and 5.5) than HYP20-C hydrogel. However, the results showed that HYP20-C hydrogel at pH = 7.4 was degraded more quickly (31.62 ± 5.82 %) than at pH = 5.5 (16.27 ± 6.80 %), after the first 10 min.

3.4.3. Spreadability test of hydrogels

Spreadability is an important property of topical formulations. To evaluate the spreadability of HYP20 and HYP20-C hydrogels, the average spreadability of 0.5 g for each hydrogel was studied after to be pressed with different weight (20, 50, 100, 200 and 500 g) every 1 min. Perpendicular diameters of the spread sample circles were measured in millimeter and taken as comparative values for spreadability (Fig. 5). The spreadability of HYP20 and HYP20-C hydrogels at 37 °C showed an average spreadability under the effect of 500 g weight pressure (104.68 ± 5.73 cm^2 and 113.95 ± 2.24 cm^2, respectively) non-significant with respect to the presence of MSCs in the hydrogel. However, the test the hydrogels at 25 °C determined that the HYP20-C hydrogel showed greater area of spreadability than HYP20 hydrogel (128.30 ± 0.69 cm^2, 94.41 ± 5.12 cm2, respectively). Concurrently, an increase in temperature from 25 °C to 37 °C significantly impacted the spreadability of the HYP20-C hydrogel (p = 0.0004), reducing it from 128.30 ± 0.69 cm2 to 113.95 ± 2.24 cm2. In contrast, for the HYP20 gel, the change in spreadability was not significant (p = 0.0816).

3.4.4. Rheological analysis

From the Fig. 6 and Table 2 it can be observed that the HYP20 and HYP20-C hydrogels are thermosensitive as expected, given that they are based on Pluronic hydrogel.

The elastic G′ and viscous G″ moduli are both important rheological parameters for poloxamer-based formulations (Liu et al., 2017b). HYP20 and HYP20-C hydrogels exhibited a liquid state (very fluid) at 4 and 10 °C, and for this reason, these systems were predominantly viscous (G″ > G′). When the temperature was increased the values of both moduli sharply increased, but with different intensities from 20 °C for HYP20-C and 19 °C for HYP20. In all cases, a crossover (G′ = G″) of 15.70 and 35.91 Pa appeared at 21.14 °C and 19.92 °C for HYP20-C and HYP20, respectively. These temperatures could be considered as the gelation point of each sample. Following this, the systems thickened considerably and became predominantly elastic (G′ > G″), exhibiting an elastic plateau from approximately 27 °C in the case of the HYP20 hydrogel. Fig. 6 shows the viscoelastic properties of both HYP20 and HYP20-C hydrogels were quite similar at low temperatures (below 18–19 °C); however, the gelation process appeared slightly delayed and more progressive for the HYP20-C hydrogel, indicating an interference effect

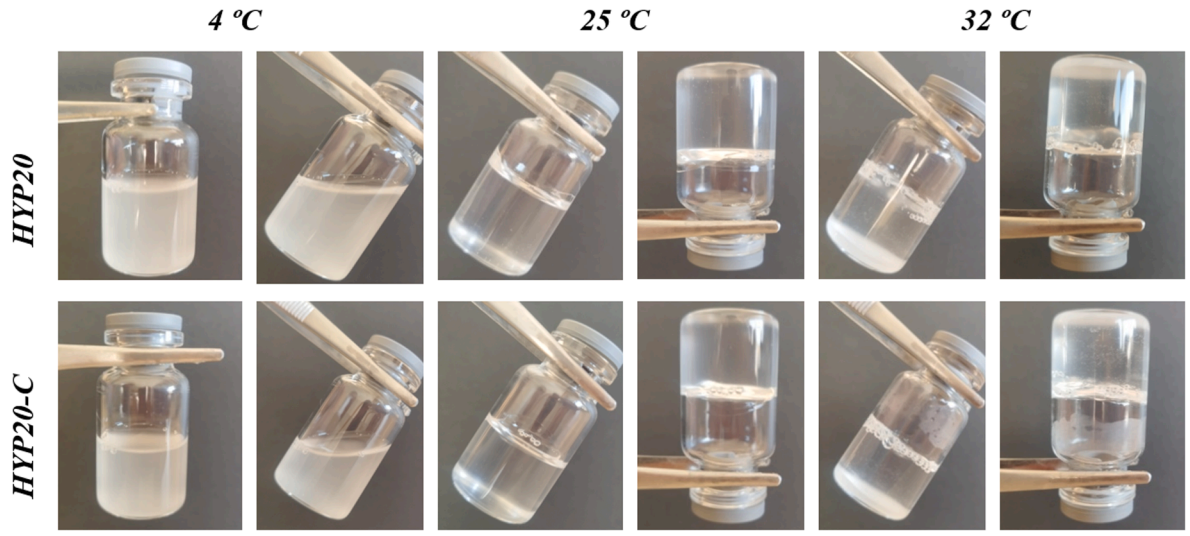

Fig. 3. Test tube inversion at 4°, 25° and 32 °C.

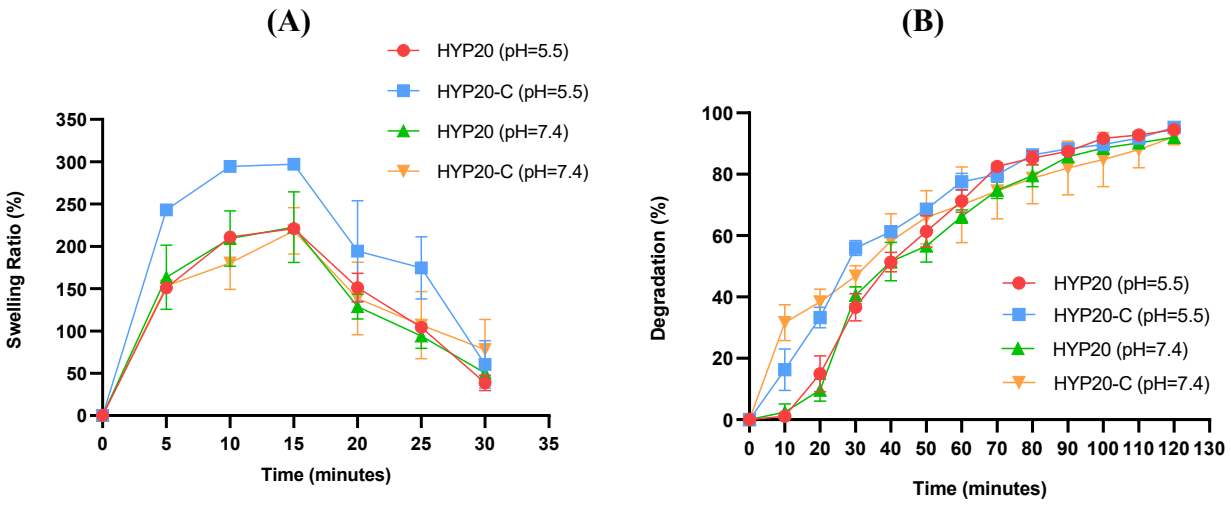

Fig. 4. Swelling and Degradation of hydrogels. (A) Swelling ratio percentage of hydrogels at pH = 5.5 and pH = 7.4 at 37 °C after 30 min. (B) Degradation percentage of hydrogels at pH = 5.5 and pH = 7.4 at 37 °C after 120 min. Values represent mean ± SD (n = 3).

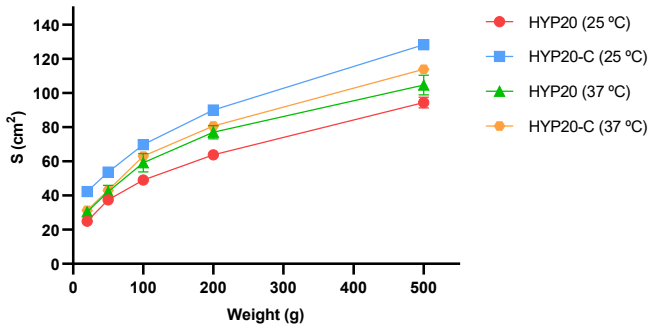

Fig. 5. Spreading area (S, cm^2) as function of the applied mass (g) at 25° and 37 °C of hydrogels. Values represent mean ± SD (n = 3).

of the cells in the structuration of the hydrogel during the gelation process.

Under rotational testing, the HYP20 and HYP20-C hydrogels exhibited non-Newtonian behavior (Fig. 7 and Table 3), displaying a pseudoplastic profile consistent with Cross's equation. However, once gelled, the hydrogels exhibited significant resistance to flow, particularly noticeable in the case of the cell-free HYP20 hydrogel, as evidenced by the irregular flow curves observed at 25 °C and 37 °C. Consequently, it has not been possible to determine the specific flow type at these temperatures for HYP20 hydrogel. Furthermore, at 37 °C, the flow curves revealed the presence of a hysteresis loop in the rheograms, which could not be evaluated in the case of the HYP20 hydrogel either. On the other hand, during the gelation process, the increase in viscosity with temperature was noticeably lower for the HYP20-C hydrogel compared to the HYP20 hydrogel. This finding confirms that the addition of cells interfered with the gelation process of the Pluronic-based hydrogel.

3.4.5. Porosity analysis

The porosity analysis was carried out by immersion of the HYPC20 hydrogel and HYP20-C in PBS (pH = 7.4 and pH = 5.5) at room temperature. The calculation of porosity resulted in values of 36.47 ± 0.74 % for HYP20 and 41.44 ± 4.19 % for HYP20-C at PBS = 7.4. Similar porosity values were obtained at pH = 5.5, the HYP20 hydrogel showed a porosity of 38.09 ± 1.40 % and the HYP20-C hydrogel exhibited a porosity of 41.35 ± 2.16 %. The values were higher at pH = 5.5 for both HYP20 hydrogel and for HYP20-C hydrogel. Besides, HYP20-C hydrogel exhibited higher porosity when compared with those of HYP20 hydrogel under the same conditions.

3.4.6. Contact angle of hydrogels

The contact angle is a way of measuring the wettability of the hydrogels surface, indicating their hydrophilic or hydrophobic characteristics. The wettability of HYP20 and HYP20-C hydrogels was evaluated at an initial time (1 min) to the final time (10 min). The measurement of contact angle for the HYP20 and HYP20-C hydrogels decreased from 30.87° to 1.31° and 31.88° to 5.69° respectively after 10 min. The wettability for HYP20-C hydrogel slightly higher than HYP20 (Fig. 8). Although the well-known hydrophilic character of Pluronic 127, This test was carried out to confirm the hydrophilic properties of the developed cells-loaded hydrogel and was recorded as a measure of wettability.

3.4.7. Conductivity

Conductivity values for HYP20 and HYP20-C hydrogels were 333.83 ± 5.85 μS/cm and 270.33 ± 2.94 μS/cm at pH = 5.5 and 311.17 ± 2.93 μS/cm and 259.83 ± 4.12 μS/cm at pH = 7.4, respectively.

3.4.8. Zeta potential of hydrogels

Measurements of zeta potential (ζ) derived from photon correlation spectroscopy are shown in Fig. 9. Cells-laden hydrogel (HYP20-C) and cells-free hydrogel (HYP20) were analyzed at different pH's ranging from 4 to 8 after 24 h. The ζ of HYP20 and HYP20-C hydrogels showed a significant variation. The ζ showed a dependence on pH. The ζ (in absolute value) followed an increase as pH increased, from 5.83 ± 0.68 mV to −11.00 ± 1.67 for HYP20 hydrogel and from 0.36 ± 0.28 mV to −12.32 ± 1.95 mV for HYP20-C hydrogel, respectively. At neutral pH, both hydrogels showed a negative zeta potential (-7.77 ± 1.09 mV from HYP20 and −10.03 ± 0.85 mV from HYP20-C) and at pH 8 any significant change was observed (-10.99 ± 1.67 mV from HYP20 and −12.31 ± 1.95 mV from HYP20-C). The point of zero charge (PZC) for HYPC20 was observed at around pH 4.6 and from HYP20-C at pH 4.

3.4.9. Leakage test

In *vitro* experiments were carried out to compare the behaviour of the gels, mimicking their topical application. To investigate leakage, which should be minimal to ensure prolonged action, the running distance of the gels over a vertical plane was measured under application on agar slides at different conditions. In Fig. 10 is depicted the running distance of HYP20 and HYP20-C hydrogels at different pH and temperatures. No differences were observed between the same sample at different pH media and at 4 and 25 °C. HYP20 exhibit greater leakage values at 37 °C

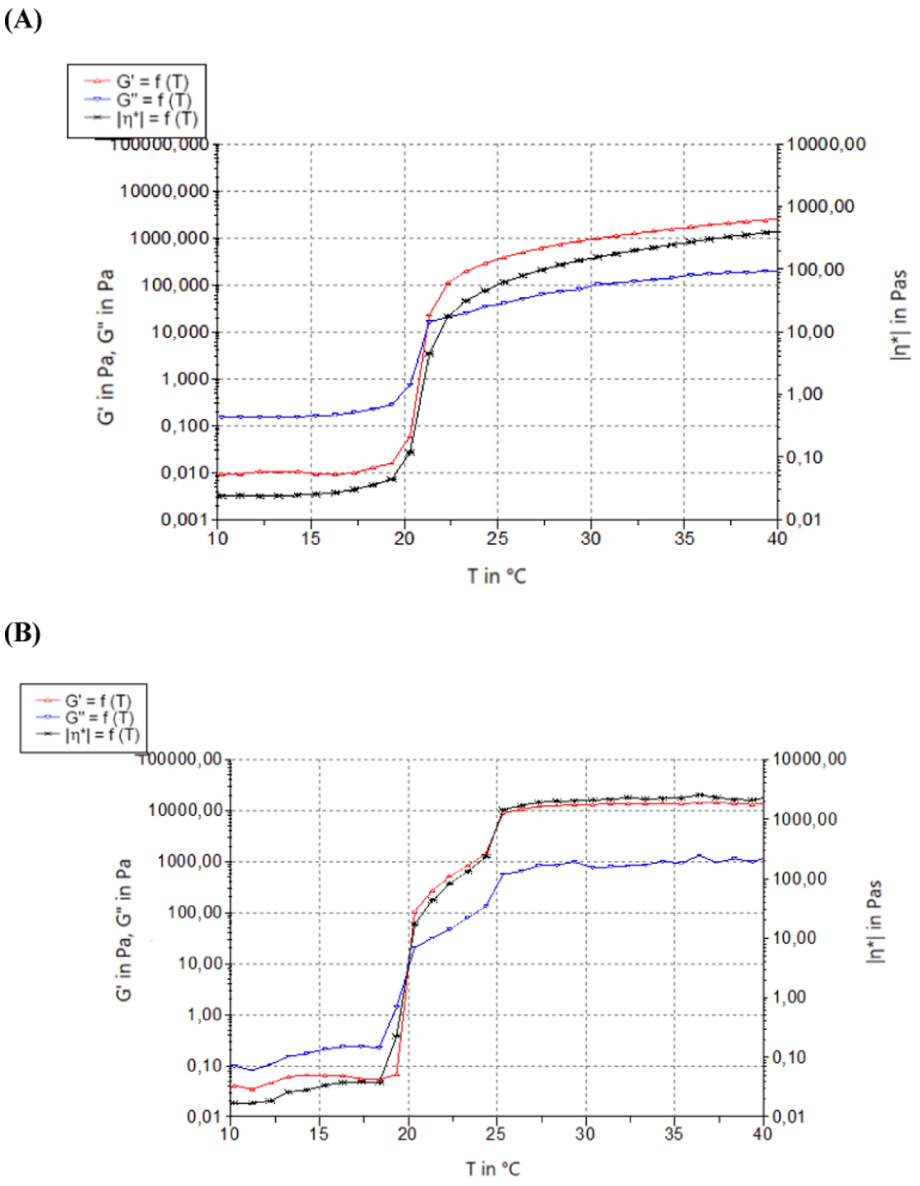

Fig. 6. Variation versus temperature of elastic modulus G′, viscous modulus G″ and complex viscosity η*, upon oscillation conditions (frequency of 1/s and shear stress of 0.5 Pa). (A) HYP20-C hydrogel and (B) HYP20 hydrogel.

Table 2
Results of the rheological oscillatory test of the hydrogels.

Formulation	Temperature (°C)	G′ (Pa)	G″ (Pa)	η* (Pa·s)
HYP20 hydrogel	10	0.041	0.099	0.017
	25	9005	564.6	1436
	37	14,280	958.4	2277
HYP20-C hydrogel	10	0.009	0.150	0.024
	25	385.1	40.23	61.62
	37	2036	180.3	325.3

and at pH 5.5 than those observed in HYP20C. Moreover, no differences were detected between HYP20 and HYP20-C at 37 °C and pH 7.4.

3.4.10. Evaluation of bioadhesion properties

Bioadhesive strength of the formulations are show in Fig. 11. It can be seen that the highest bioadhesive force values were obtained at 37 °C for both formulations. HYP20 hydrogel exhibited value at 32 and 37 °C of 47.82 ± 8.77 mN/cm^2 and 119.98 ± 1.88 mN/cm^2, respectively. HYP20-C hydrogel exhibited values of 81.08 ± 3.54 mN/cm^2 at 32 °C and 94.73 ± 3.44 mN/cm^2 at 37 °C.

The bioadhesive property was also evaluated measure the influence of the samples on the zeta potential of mucin. It was observed that the ζ value of the mucin solution, −10.58 ± 0.77 mV, changed when mixed it with the hydrogels, became more positive. The ζ values of the hydrogels were −2.65 ± 0.53 mV and −5.56 ± 0.51 mV for mucin-HYP20 and mucin-HYP20-C, respectively.

3.4.11. Extrudability study

The results of extrudability can be observed in Table 4. As might be expected, HYP20-C hydrogel is the sample that extrudes most easily. It can be seen that the highest extrudability values were obtained at 25 °C for both formulations, indicating that are require the maximum force to be extruded from the syringe. Furthermore, it can be observed that extrudability decreases with increasing syringe volume in all temperatures assayed and in both formulations.

3.4.12. Spray angle

In Fig. 10B is depicted the spray angle of HYP20 and HYP20-C hydrogels at different temperatures. The average spray angle produced

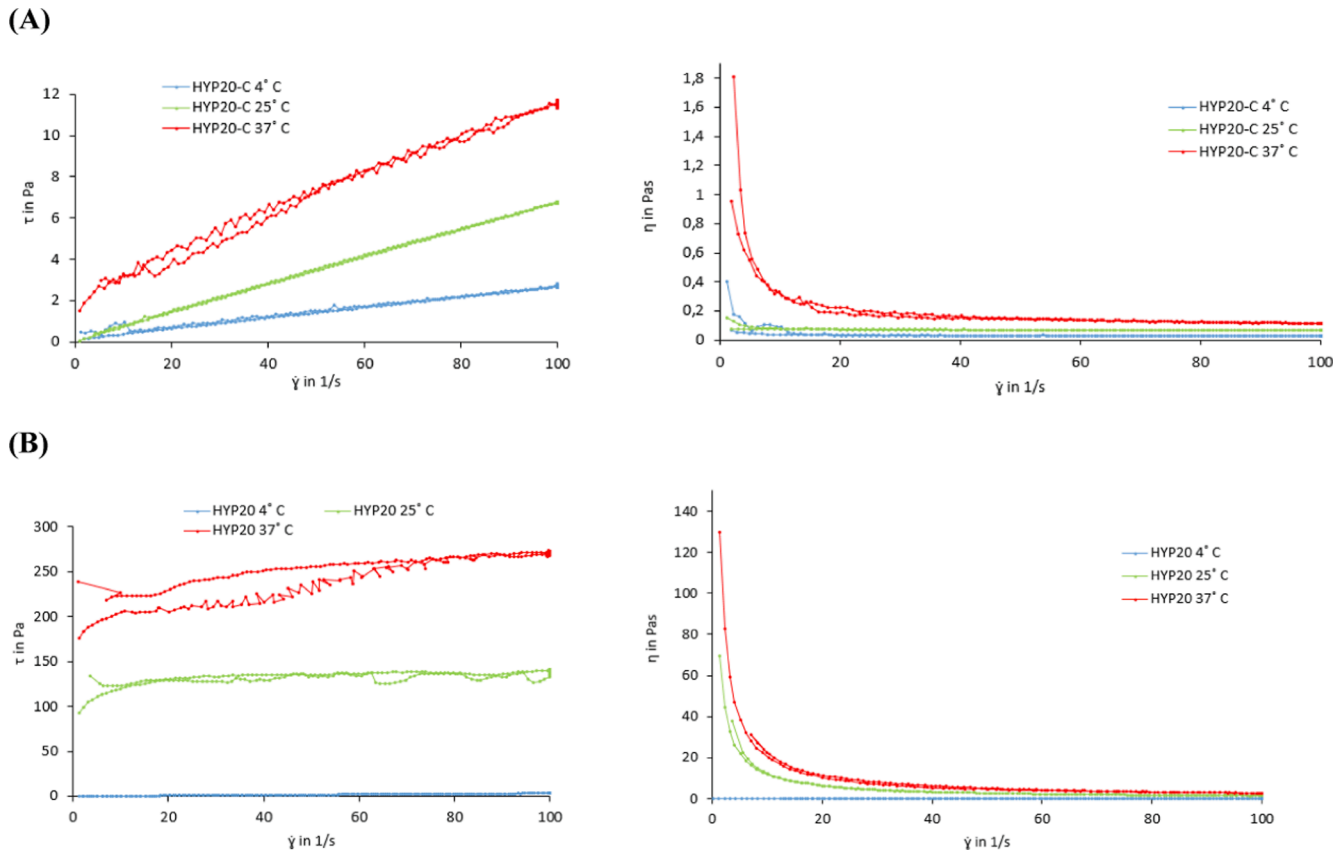

Fig. 7. Variation versus temperature of the flow curve ($\tau = f(\dot{\gamma})$) and viscosity curve ($\eta = f(\dot{\gamma})$), upon rotational conditions. (A) HYP20-C hydrogel and (B) HYP20 hydrogel.

Table 3
Results of the rheological rotational testing of the HYP20 and HYP20-C hydrogels.

Formulation	Temperature (°C)	Rheological behavior and Mathematical Model Fitting		Viscosity at 100 s^{-1} (Pa·s)	Hysteresis loop area (Pa/s)
		Ramp-Up Stretch	Ramp-Down Stretch		
HYP20-C hydrogel	4	Pseudoplastic Cross, r = 0.9988	Pseudoplastic Cross, r = 1.0000	0.027 ± 0.31	No hysteresis loop
	25	Pseudoplastic Cross, r = 1.0000	Pseudoplastic Cross, r = 1.0000	0.068 ± 0.11	No hysteresis loop
	37	Pseudoplastic Cross, r = 0.9957	Pseudoplastic Cross, r = 0.9986	0.115 ± 0.81	No hysteresis loop
HYP20 hydrogel	4	Pseudoplastic Cross, r = 1.0000	Pseudoplastic Cross, r = 1.0000	0.032 ± 0.05	No hysteresis loop
	25	Non-Newtonian	Non-Newtonian	1.379 ± 19.94	Hysteresis loop detected, but cannot be evaluated
	37	Non-Newtonian	Non-Newtonian	2.706 ± 22.19	Hysteresis loop detected, but cannot be evaluated

showed a dependence on temperature and followed a decrease as temperature increased from 4 to 25 °C, from 5.8 ± 0.20 ° to 3.21 ± 0.22 ° for HYP20 hydrogel and from 7.59 ± 0.07 ° to 3.15 ± 0.34 ° for HYP20-C hydrogel.

3.4.13. Differential scanning calorimetry (DSC) and thermogravimetric analysis (TGA)

The thermal behavior of fresh HYP20 hydrogel and freeze-dried HYP20 hydrogel was evaluated by Thermogravimetric Analysis and Differential Scanning Calorimetry. TGA is a method of thermal analysis in which the mass of a sample is measured over time as the temperature changes. The method makes it possible to study those physical changes such as phase transition, absorption and desorption, as well as chemical reactions including thermal decomposition, accompanied by a change in mass (Ramos, 2022). The thermal degradation profiles of the hydrogels showed small differences related to the presence of the water, as seen in Fig. 12. To the fresh HYP20 hydrogel, the first weight loss occurred at 30–140 °C, with a weight loss percentage of 79.9 % (Fig. 12**A**). In contrast, in freeze-dried hydrogel a minimal weight loss (5.72 %) can be observed approximately at 30–167 °C possibly due to residual moisture (Fig. 11b). A gradual loss of mass is observed in the temperature ranging from 140 to 322 °C for fresh HYP20 hydrogel, which is not observed in the freeze-dried HYP20. Furthermore, the second major degradation event took place from 330 to 420 °C in both hydrogels, which can be associated with the polymer thermal decomposition. Finally, at the end of the thermal curve of fresh HYP20 hydrogel and freeze-dried HYP20 hydrogel, was detected a loss weight of 0.28 mg in the temperature ranging from 420 to 756 °C and 0.74 mg from 420 to 870 °C, respectively.

The thermal study was completed by also performing a DSC analysis

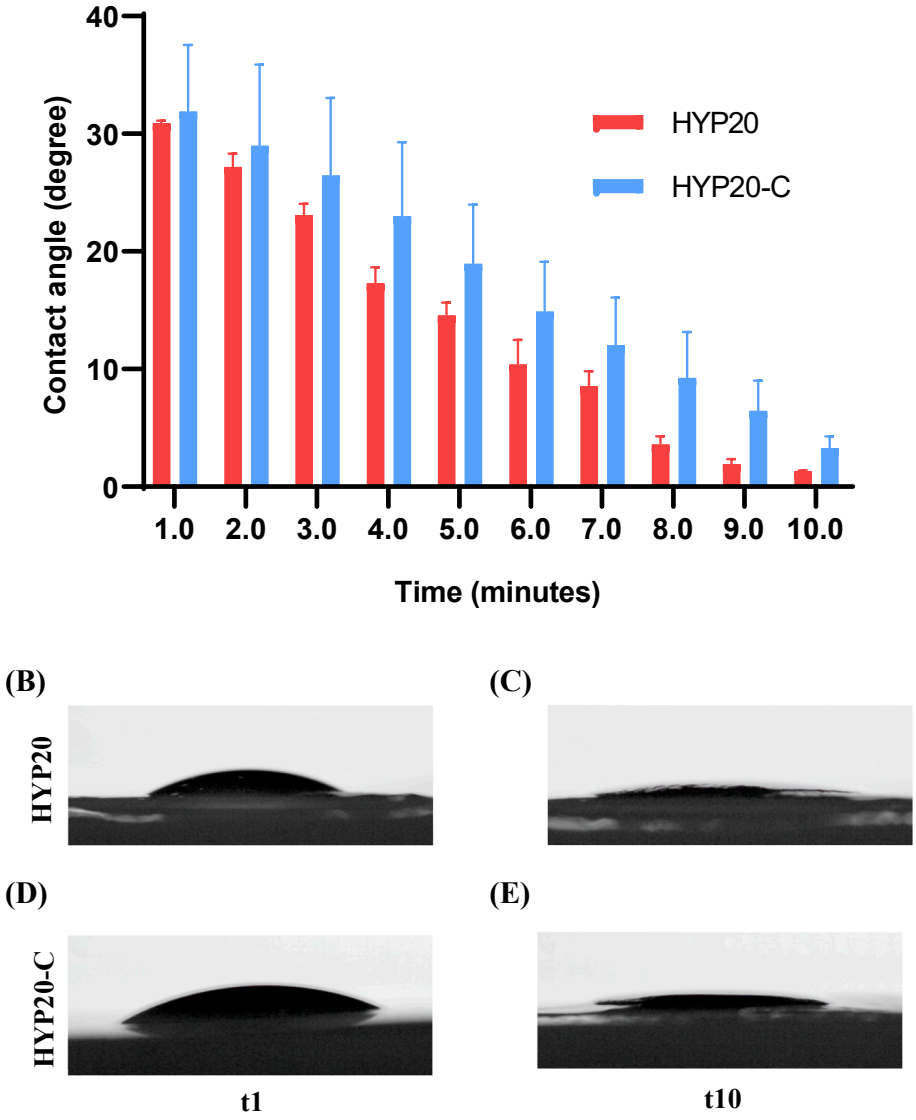

Fig. 8. (A) Contact angle of HYP20 and HYP20-C hydrogel an initial time (1 min) to the final time (10 min). (B) Contact angle of HYP20 hydrogel at 1 min. (C) Contact angle of HYP20 hydrogel at 10 min. (D) Contact angle of HYP20-C hydrogel at 1 min. (E) Contact angle of HYP20-C hydrogel at 10 min.

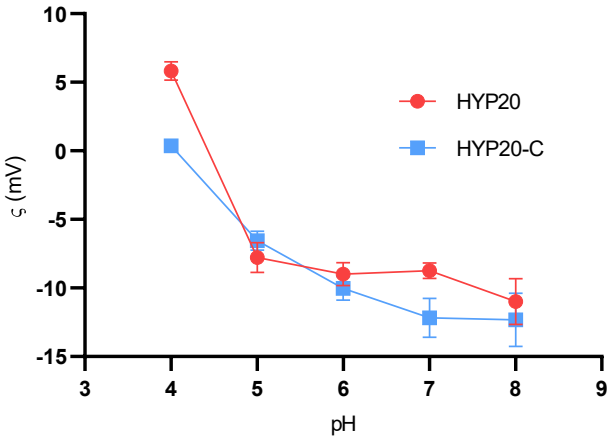

Fig. 9. Zeta potential (ζ, mV) of HYP20 and HYP20-C hydrogels as a function of ionic as a function of pH in the presence of 10^{-3} M KNO_3 concentration at 25 °C. Values represents the mean ± SD (n = 9).

of the samples studied. This technique is a useful tool for investigating temperature-induced transitions in thermosensitive polymer solutions (Hirun et al., 2022). The DSC thermograms are shown in Fig. 13. As can see in Fig. 13**A**, in fresh HYP20 hydrogel endothermic peak was observed at 94 °C, which corresponded to first weight loss. The second endothermic peak was observed at 370 °C corresponding to the degradation of polymer observed above, in the TGA. In contrast, in freeze-dried HYP20 hydrogel endothermic peak was observed at 60 °C, due to a phase change of the polymer (Fig. 13**B**). The second endothermic peak was observed at 373 °C also due to polymer degradation.

The DSC thermogram has also been recorded in the temperature range from 0 to 60 °C (Fig. 14) to order to observe the sol–gel transition. The micellization process is a spontaneous process that begins when the concentration of the copolymer in solution reaches the critical micellar concentration (CMC) at a fixed temperature or by increasing the temperature to the critical micellar temperature (CMT) at a fixed copolymer concentration (Linse, 1993). Below the CMC, unimeric copolymers are dispersed in water. Once the CMC is exceeded, micelle formation occurs. Fig. 14 shows the occurrence of an intense and broad peak centered, possibly ascribed to micellar formation process (Boonlai et al., 2017). At 12 °C, a phase transition is observed (the sol–gel transition) which is

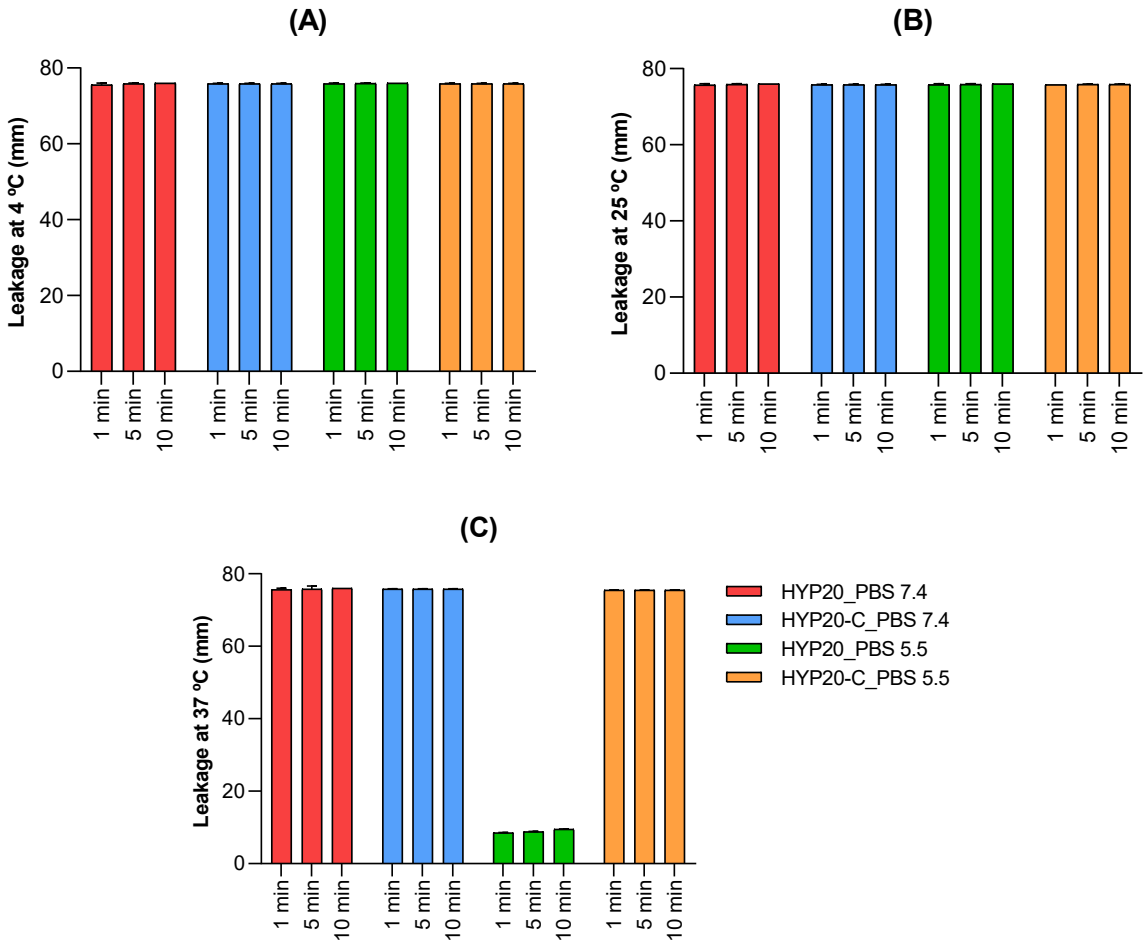

Fig. 10. Leakage (mm) of hydrogels after 1, 5 and 10 min, in agar surface at different conditions; (A) Leakage at pH 7.4 and pH 5.5 at 4 ± 0.5 °C (A; B) Leakage at pH 7.4 and pH 5.5 at 25 ± 0.5 (C) Leakage at pH 7.4 and pH 5.5 at 37 ± 0.5 Bars represent mean ± SD (n = 3).

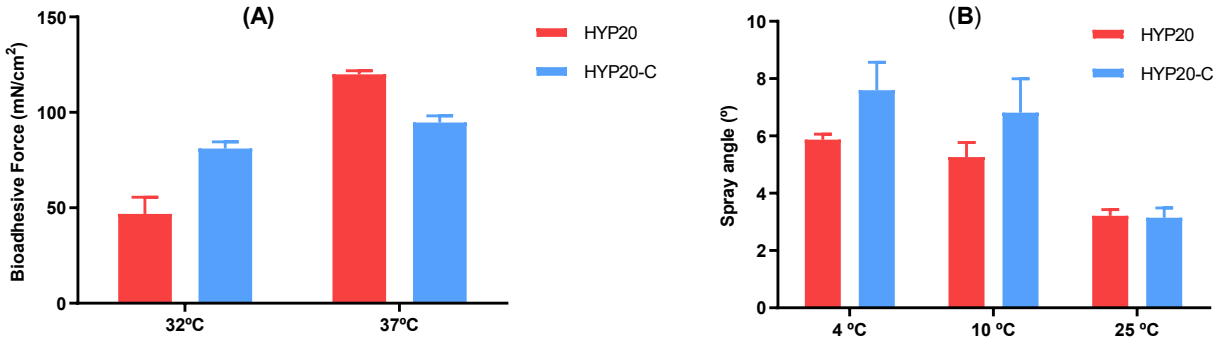

Fig. 11. (A) Bioadhesive force (mN/cm^2) of hydrogels in pig skin. (n = 3). (B) Spray angle (°) of formulations at 4, 10 and 25 °C. Results are expressed as mean ± SD.

considered complete at 14 °C. At this temperature, the PPO blocks of P407 become dehydrated and subsequently associate upon heating. The assembly of the dehydrated poloxamer 407 blocks causes the micelle formation giving rise to the gel. The gel is the result of a phase transition from the sol state, or micellar solution, to a solid cubic micellar state (Bodratti and Alexandridis, 2018; de Castro et al., 2023).

3.5. Morphological characterization

3.5.1. Size

Mean particle diameter and PdI of hydrogels were analyzed by photon correlation spectroscopy at different temperatures. The results of Table 5 show an increase in size as temperature increased from 5.06 ± 1.28 to 17.54 ± 0.84 nm and 5.32 ± 0.69 nm to 19.28 ± 0.81 nm for HYP20 and HYP20-C, respectively. Thus, no significant differences in size were observed after cell incorporation.

3.5.2. Environmental scanning electron microscopy analysis

Fig. 15 shows SEM photographs of HYP20 and HYP20-C hydrogel, demonstrating that hydrogels possess high porosity and interconnected pores. It was also observed a relatively homogeneous pore size distribution around 7–9 μm and 6–8 μm for HYP20 and HYP20-C, respectively.

The hydrogel was also examined using the critical point drying

Table 4
Extrudability (g/m^2) behavior at 4 and 25 °C of HYP20 and HYP20-C hydrogels. Each value represents the mean ± SD (n = 3).

Formulation	Temperature (°C)	Syringe (ml)	Extrudability (g/cm^2)
HYP20	4	2	12.18 ± 1.83
		5	3.53 ± 0.50
		10	2.77 ± 0.10
	25	2	46.17 ± 7.69
		5	14.86 ± 2.42
		10	4.85 ± 0.33
HYP20-C	4	2	7.11 ± 2.75
		5	2.58 ± 0.72
		10	2.02 ± 0.27
	25	2	16.23 ± 1.27
		5	6.66 ± 0.64
		10	2.24 ± 0.06

technique, as shown in Fig. 16. The analysis revealed a network with an interconnected porous structure, which is derived from the potential cubic self-assembly micellar disposition typical of poloxamer.

3.5.3. *Lyophilization and relationship with the extrusion process*

The SEM images of the lyophilized hydrogels reveal porous structures with agglomerated irregular pore sizes resulting from the removal of water during freeze-drying, which causes the interconnected networks within the hydrogel to stack (Fig. 17). Micrographs were similar for the HYP20 and HYP20-C hydrogels, both at 4 °C and 25 °C, extruded and non-extruded. Thus, the extrusion process did not change the morphology of the hydrogels.

3.6. *Wound-healing assay*

The mechanical damage to confluent cell layers, as known as scratch wound healing assay, is one of the most extensively researched *in vitro* models for studying wound healing that allows high-throughput quantification of wound closure by keratinocytes (Jaramillo et al., 2023; Shin et al., 2023; Wiegand et al., 2021; Yu et al., 2023). HEKa keratinocytes (Fig. 18) were investigated as model cells for dermal wound healing**.** The measurement of the wound area of the keratinocyte layer was studied after 4 h treatment with the different concentrations of hMSCs in the hydrogel. In the absence of hMSCs, HYP20 hydrogel a reduction in the wound area of the keratinocyte layer of approximately 65 % was observed. This reduction was similar to that of the lowest and the middle concentration of the HYP20-C. However, at the highest concentration assayed, the wound area was completely closed.

To further study the effect of the HYP20-C at the highest concentration, an insert was used to remove the hMSCs from the surface of the layer (there were only HEKa cells in the well, and only HYP20-C hydrogel in the insert). Interestingly, at 4 h the wound area was practically the same with only a 4.87 % reduction (±2.1 %), indicating that for a better healing, the HYP20-C needed to be applied directly. When cells were not in contact, the wound area was not closed at 4 h; the closure was even lower than with the lowest concentration of dermal stem cells. Moreover, after 19 h all conditions assayed had fully recovered the presence of keratinocytes at the wound, suggesting that the HYP20-C did not cause any damage to the cell layer and was useful to ameliorate the wound healing.

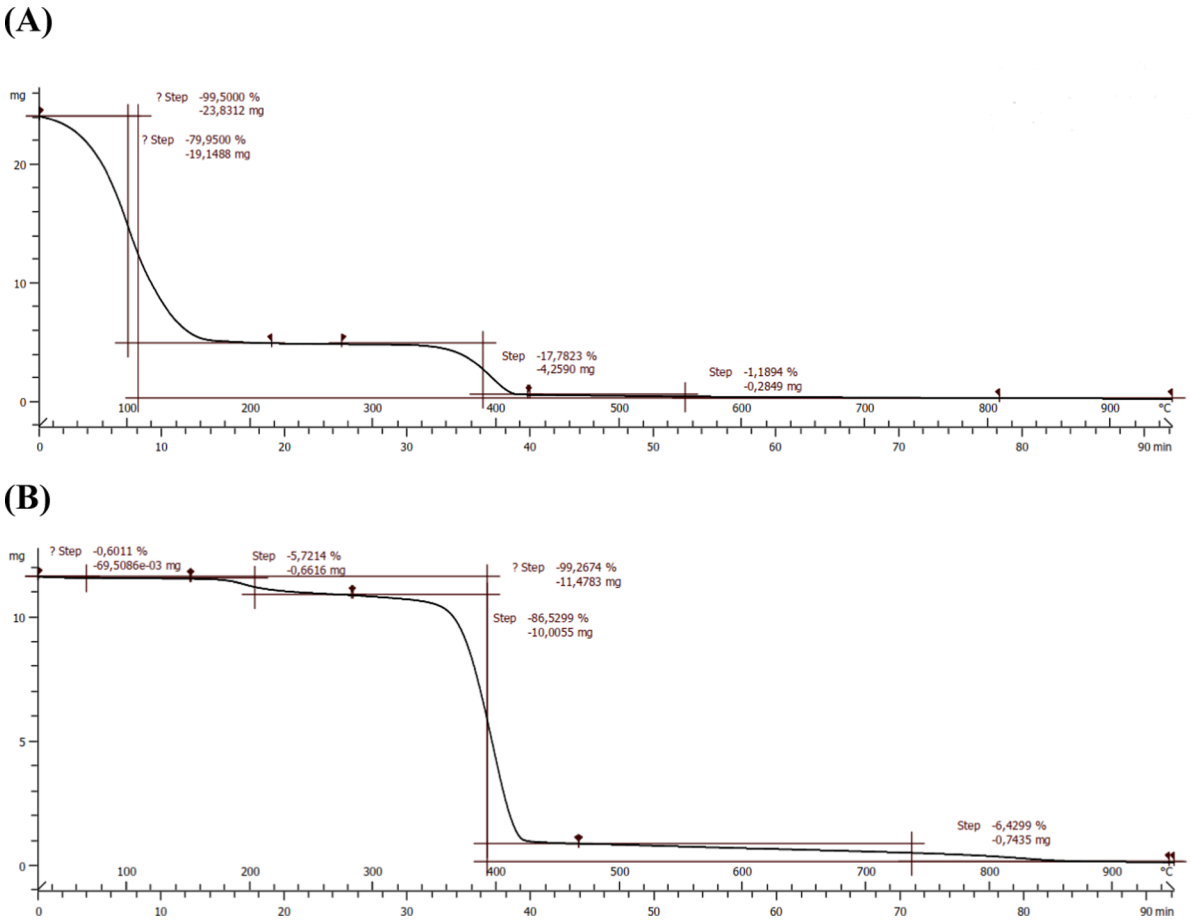

Fig. 12. (A) TGA thermogram of fresh HYP20 hydrogel and (B) TGA thermogram of freeze-dried HYP20 hydrogel in the temperature range from 28 to 950 °C.

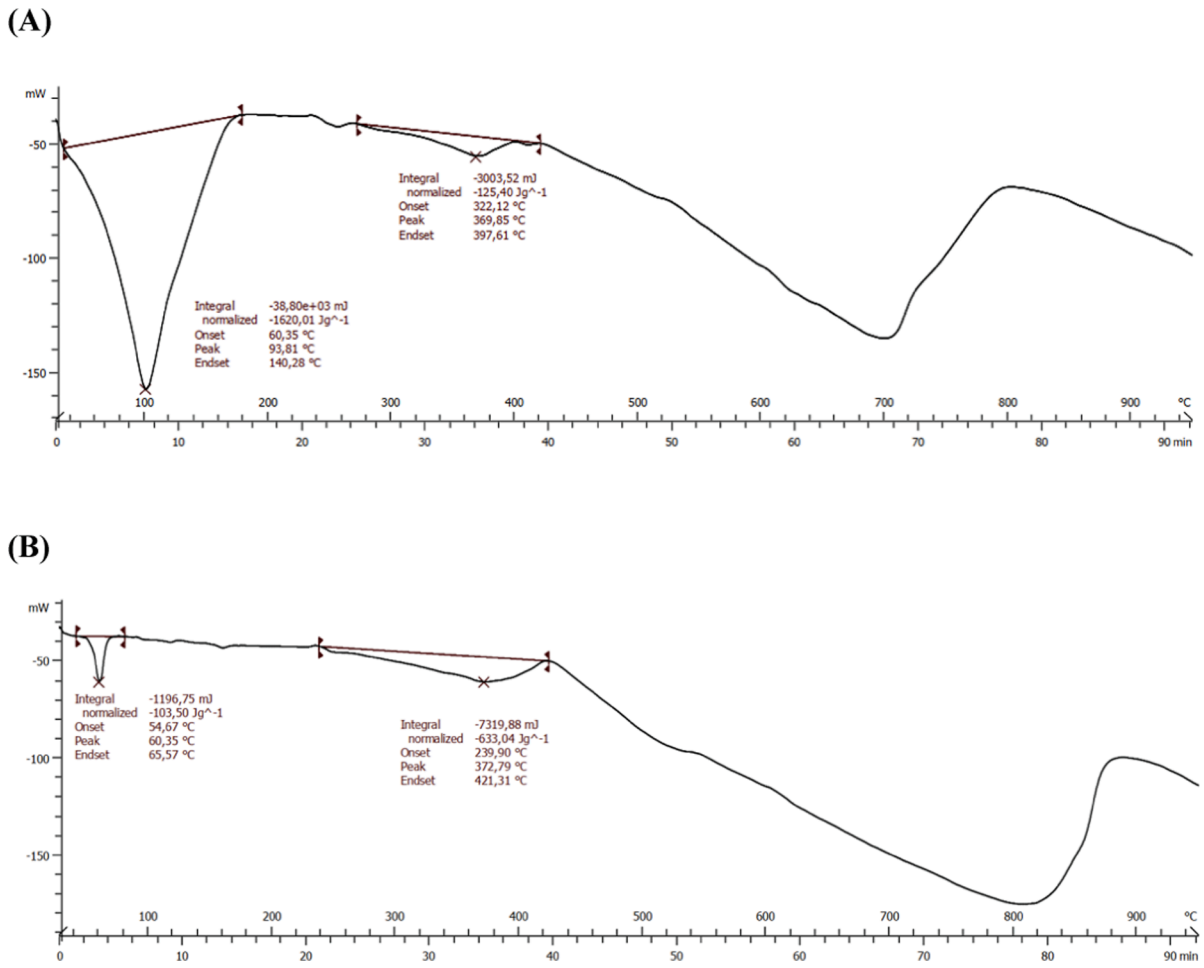

Fig. 13. (A) DSC thermogram of fresh HYP20 hydrogel in the temperature range from 28 to 950 °C. (B) DSC thermogram of freeze-dried HYP20 hydrogel.

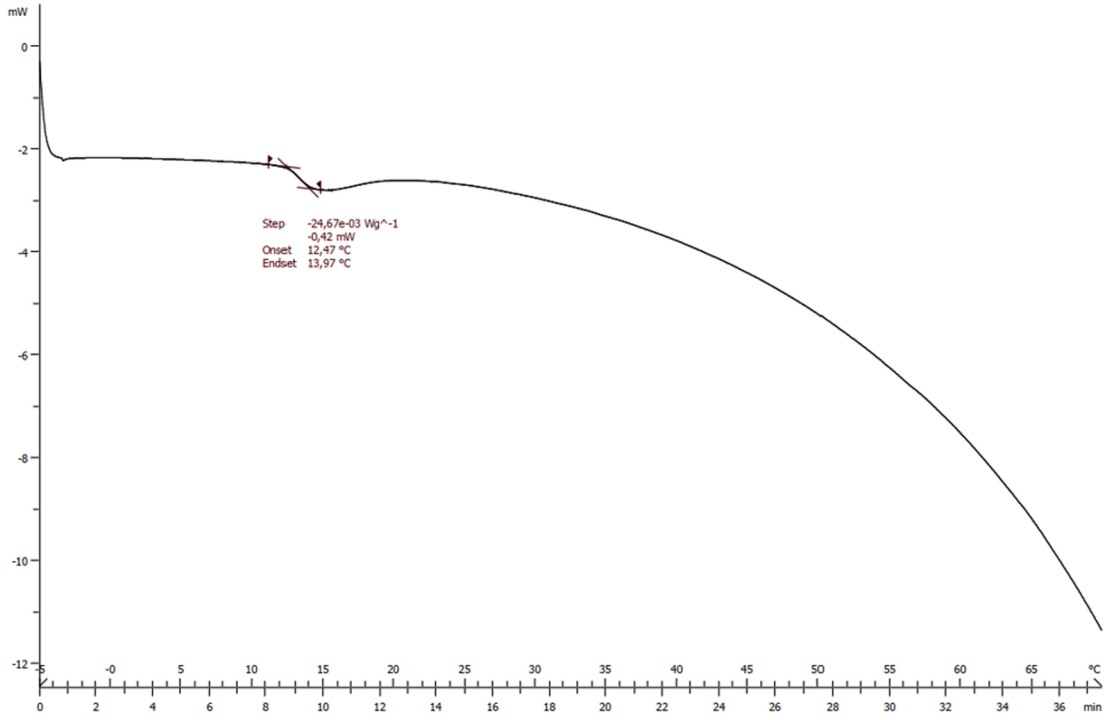

Fig. 14. DSC thermogram fresh HYP20 hydrogel in the temperature range from −5 to 70 °C.

Table 5
Mean particle diameter and PdI of hydrogels at 4, 32 y 37 °C. The data are expressed as mean ± standard deviation (SD) of three replicates (n = 3).

Formulation	Temperature (°C)	Size (nm)	PdI
HYP20	4	5.06 ± 1.28	1.28 ± 0.65
	32	16.28 ± 1.83	0.45 ± 0.41
	37	17.54 ± 0.84	0.20 ± 0.02
HYP20-C	4	5.32 ± 0.69	0.90 ± 0.12
	32	16.21 ± 1.15	0.28 ± 0.08
	37	19.28 ± 0.81	0.41 ± 0.10

4. Discussion

After testing a wide range of concentrations, the developed hydrogel based on 20 % (w/w) Pluronic (HYP20-C) resulted the optimal formulation, in terms of biocompatibility, optical and gelling properties. Results from Trypan Blue assay indicated that all formulations exhibited good cell viability, as expected provided that poloxamer is approved by FDA to be used in many biomedical areas (FDA, 2023). Our study also confirmed that the polymer is able to support high cell survival even at high concentrations (Alvarado-Gomez et al., 2018; Fedorovich et al., 2009; Khattak et al., 2005; Oshiro et al., 2014). Our results also corroborate others reporting that Pluronic could only jellify at the concentration of 20 % (w/w) (Escobar-Chávez et al., 2006; Lenaerts et al., 1987; Matthew et al., 2002; Oshiro et al., 2014). Moreover, this concentration was successfully used for *in vivo* applications (Arévalo-Silva et al., 2000; Cao et al., 1998). Low cytotoxicity of HYP20-C hydrogel was also confirmed by Live/Dead assay, showing a high number of living cells in solution state (at 4 °C) and in gel state (at 37 °C) up to 48 h, in accordance to previous studies (Fedorovich et al., 2009; Khattak et al., 2005; Oshiro et al., 2014). However, it decreased significantly after 72 h in gel state, attributed to the detrimental effect on cell membrane integrity, potentially associated to the increase in the osmotic pressure of the environment and/or to the inert properties of Pluronic (Fedorovich et al., 2009; Khattak et al., 2005; Nuttelman et al., 2005; Stupack and Cheresh, 2002), that led to keep the cells in a round morphology over an extended period of time. This problem could be solved by the addition of membrane stabilizers (e.g., hydrocortisone or glycerol) to the HYP20-C formulation and/or components with bioactive segments (e.g., RGD), as demonstrated other authors (Fedorovich et al., 2009; Khattak et al., 2005; Shachaf et al., 2010). Besides this, detrimental effects of F127 have not been documented *in vivo*, since its half-life is much lower (≈21 h) than it is *in vitro* (Johnston et al., 1992; Khattak et al., 2005). It indicates that HYP20-C formulation would be likely cleared before affecting significantly cell viability and, therefore, it could be successfully applied as a wound dressing.

The gelation is a reversible process and is recognized by a sol–gel transition temperature (Tsol-gel). Poloxamer 407 aqueous solutions remain fluid below Tsol-gel and above this temperature turn to a semi-solid (Dumortier et al., 2006; Fakhari et al., 2017). Gelation results from hydrophobic interactions between Poloxamer 407 copolymer chains. As the temperature increases, the copolymer chains of poloxamer 407 aggregate into a micellar structure. Formation of micelles results from dehydration of the hydrophobic PPO repeating units and defines the initial step of gelation (Dumortier et al., 2006; Fakhari et al., 2017). Our results our results showed that the addition of MSCs slightly decreased the Tsol-gel.

Osmolality is an important factor in the design of a hydrogel for cell delivery in wound healing (Sivaraj et al., 2021). It is essential for cell survival due to favor oxygen and nutrient diffusion (Perez-Valle et al., 2020). These values should be similar to physiological osmolality (approximately 300 mOsm/kg) (DiBartola, 2012), as cells can die if resuspended in a non-physiological polymeric solution (Zhao et al., 2021). Hypoosmolality induces cell swelling, whereas hyperosmolality causes cell shrinkage. Such osmotic imbalances adversely affect to cell proliferation, migration and apoptosis (Parvanian et al., 2021). The cell-loaded hydrogel showed an osmolality similar to physiological osmolality. Furthermore, no negative effects on cell behavior were identified, thus the hydrogel is adequate to ensure the cell survival.

The swelling properties in wound healing could help to adsorb exudates and offer mechanical resistance to the delivery system at the biological site of action (Soriano-Ruiz et al., 2020). To mimic the skin surface and the more internal skin tissue environment, the swelling behavior was assayed at two different pH vales. Our results showed high

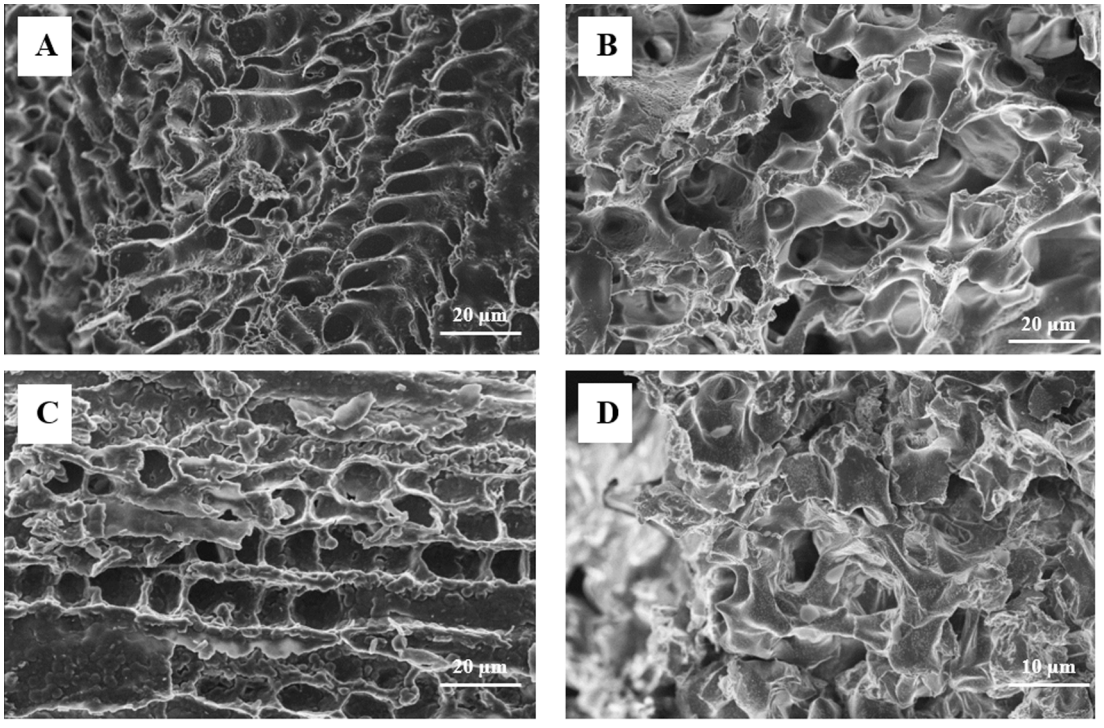

Fig. 15. Representative SEM images of HYP20 hydrogel (A, B) and HYP20-C hydrogel (C, D) in high vacuum mode.

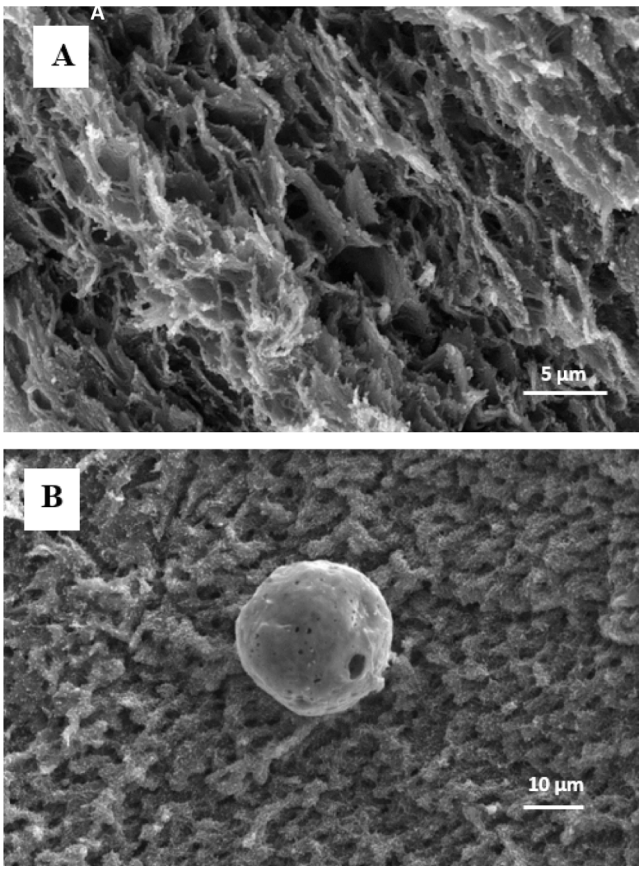

Fig. 16. SEM images of HYP20 hydrogel (A) and HYP20-C hydrogel (B) obtained by critical point drying.

rates of swelling for both hydrogels at the different pH values. The values were higher at pH = 5.5 for both HYP20 hydrogel and for HYP20-C hydrogel being HYP20-C the best formulation in this sense at pH = 5.5. The designed hydrogel exhibits excellent swelling and can absorb exudate from wounds.

The results of the degradation profile characterization showed that poloxamer 407 hydrogels degraded rapidly. The degradation of the hydrogel was lower at pH = 7.4 when compared to pH = 5.5, likely because of the higher solubilization of the hydrogel's polymeric matrix, which led to higher loss. No differences were observed between the hydrogels in any of these studies. The degradation of the hydrogel could be attributed to the penetration of the PBS solution into its three-dimensional structure, which leads to the disintegration of the cross-linking points and the weakening of the interaction among the polymer's macromolecules (Xu et al., 2020). This property makes the hydrogel a potentially candidate for the rapid release of stem cells and other sensitive bioactive molecules *in vivo* (Diniz et al., 2015).

The spreadability of hydrogels is also an important factor to evaluate in topical formulation and it is used to determine the ability of a formulation to spread when a certain force is applied, in an attempt to replicate the spreading characteristics on the skin (Batista et al., 2022). It consists on the expansion of a semi solid formulation on a surface after a certain time, under the action of a pressure of a weight, and its determination is important because topical formulations should be easy to apply on the skin surface (Semak et al., 2012). This property can affect both the packaging process and the correct administration dosage and application, and therefore its efficacy (Brugués et al., 2015; Soriano-Ruiz et al., 2019a). The efficacy of topical therapy is directly related to optimal spreadability, which also makes the product easy to apply (Soriano-Ruiz et al., 2019b). Spreadability of semi-solid forms, such as gels, arises from a combination of rheological contributions, among which viscosity is only one factor. Typically, the higher the viscosity of the semisolids, the lower the surface tension, making the product less spreadable (Szulc-Musioł et al., 2017). However, structural and viscoelastic characteristics, which describe rigidity, strength, and the balance between elastic and viscous behaviors, also play a significant role in determining spreading properties. Our results indicate that HYP20-C exhibits superior spreadability properties at 25 °C compared to 37 °C, which can be attributed to the combination of rheological contributions that includes viscosity (Szulc-Musioł et al., 2017) and structural and viscoelastic characteristics, which describe rigidity, strength, and the balance between elastic and viscous behaviors.

Rheology is a widely used technique to characterize the structural strength of semisolid systems and predict their behaviour for topical administration. Moreover, the rheological measurements showed the degree to which a sample deforms, or the rate at which it flows, when a stress is applied to the sample (Mallandrich et al., 2017; Soriano-Ruiz et al., 2019a). To simulate the behavior after storage in the refrigerator or at room temperature, and after application on the skin, sample readings were taken at 4, 25, and 37 °C. A hydrogel suitable for topical application should be free-flowing at room temperature (25 °C) and capable of transforming into a hydrogel when it comes into contact with the skin's surface physiological temperature (32 °C). This liquid formulation allows for easy application from the packaging material and better spreadability on the affected area. Upon contact with the skin's temperature, the formulation begins to thicken, enhancing retention (Pironi et al., 2022). As expected, the hydrogels under study were predominantly viscous ($G'' > G'$) at low temperature, as they are thermosensitive and remain liquid at 4 and 10 °C. The TSOL-GEL point (where $G' = G''$) was approximately 21 °C and 20 °C for HYP20-C and HYP20, respectively. This is the temperature at which hydrogels exhibits a switch from a viscous behaviour to a prevalently elastic ($G' > G''$). This interesting gelation process results in an increase in the residence time avoiding the rapid gel elimination (Giuliano et al., 2018). Both hydrogels exhibited a sol–gel phase transition at temperatures below body temperature. The results indicated that the poloxamer 407 hydrogel is suitable for use as in situ gel systems for topical administration (Pironi et al., 2022). Under rotational testing, the HYP20-C and HYP20 hydrogels displayed a non-Newtonian behavior, conforming to a pseudoplastic profile in most of the rotational tests carried out. Such characteristics are typical for systems based on poloxamer (Baloglu et al., 2011). Furthermore, during rotational testing at 37 °C, flow curves for both hydrogels revealed a structural rearrangement, as evinced by the emergence of a hysteresis loop in the rheograms. This loop typifies time-dependent viscosity changes (Lee et al., 2009). Compared to the free-cell HYP20 hydrogel, the HYP20-C hydrogel, which contains cells, showed a significant lower increase in viscosity as temperature increased, indicating a complex relationship between structural modification in the hydrogels and changes in temperature.

The degree of porosity greatly affects nutrient, metabolites and oxygen diffusion but it also promotes waste removal, influences neovascularization, cellular infiltration/migration and provides suitable growth space for tissue regeneration (Flégeau et al., 2017; Qian et al., 2020). Moreover, the porosity directly affects swelling (Ceccaldi et al., 2017; Li et al., 2019; Zielinska et al., 2023). Our results were in line with swelling results pH, according to which, the HYP20-C possessed higher porosity values. These showed that the porosity was adequate for cell infiltration.

The contact angle is a way of measuring the wettability of the material surface, indicating hydrophilic/hydrophobic characteristics of the material. In general, a contact angle less than 90° indicates a hydrophilic surface, while a contact angle larger than 90° correspond to a hydrophobic surface (Yuan and Lee, 2013). It is notice that HYP20 has a contact angle less than 90° which indicates a hydrophilic nature. The contact angle decreases with time for each hydrogel. Furthermore, HYP20 is more hydrophilic than HYP20-C; thus, the addition of MSCs decrease the surface wettability and, consequently, the contact angle

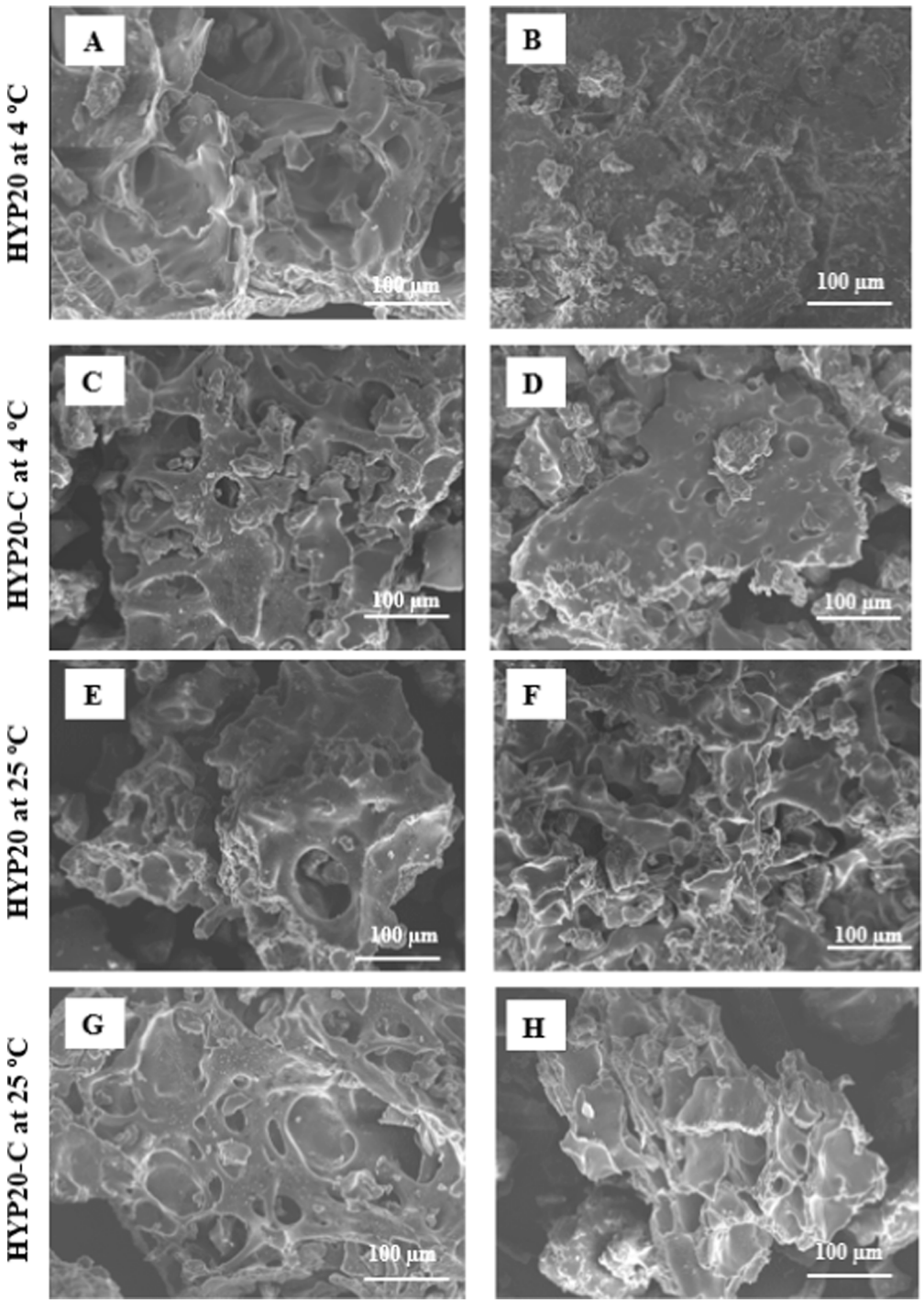

Fig. 17. Scanning electron micrographics comparison of hydrogels after simple extrusion. (A) HYP20 control at 4 °C, (B) extruded HYP20 at 4 °C, (C) HYP20-C control at 4 °C, (D) extruded HYP20-C at 4 °C, (E) HYP20 control at 25 °C, (F) extruded HYP20 at 25 °C, (G) HYP20-C control at 25 °C, (H) extruded HYP20-C at 25 °C.

increase. However, it can be observed that there are no significant differences between the contact angle values of both hydrogels. Hydrophilic properties of hydrogel can play an important role in preventing bacterial infections due to the capability of removing bacteria and inhibiting bacterial adhesion to surfaces (Fu et al., 2021; Zhao et al., 2015), in stimulating cell migration and prevention of loss of bodily fluids and essential nutrients *in vivo* (Kim et al., 2016; Pan et al., 2014). Thus, our designed hydrogel can be considered as suitable for skin wound healing.

The zeta potential can influence both static and dynamic cell behavior (Chen et al., 2011). Our results showed a negative ζ in the assayed pH range owing to the presence of hydroxyl group on the surface of poloxamer 407. Similar results of zeta potential are described in other studies (Ci et al., 2017; Liu et al., 2017a). The negative surface charge of the hydrogel can interact with cell adhesion proteins that have hydrophobic or positively charged amino acids, such as arginine and lysine (Cardin and Weintraub, 1989). The amino acids bind to integrins, which is necessary for T to trigger cell adhesion, signalling and spreading. Prior studies have shown that both cell–cell and cell-material interactions can control by a negative surface (Tripathi and Melo, 2015).

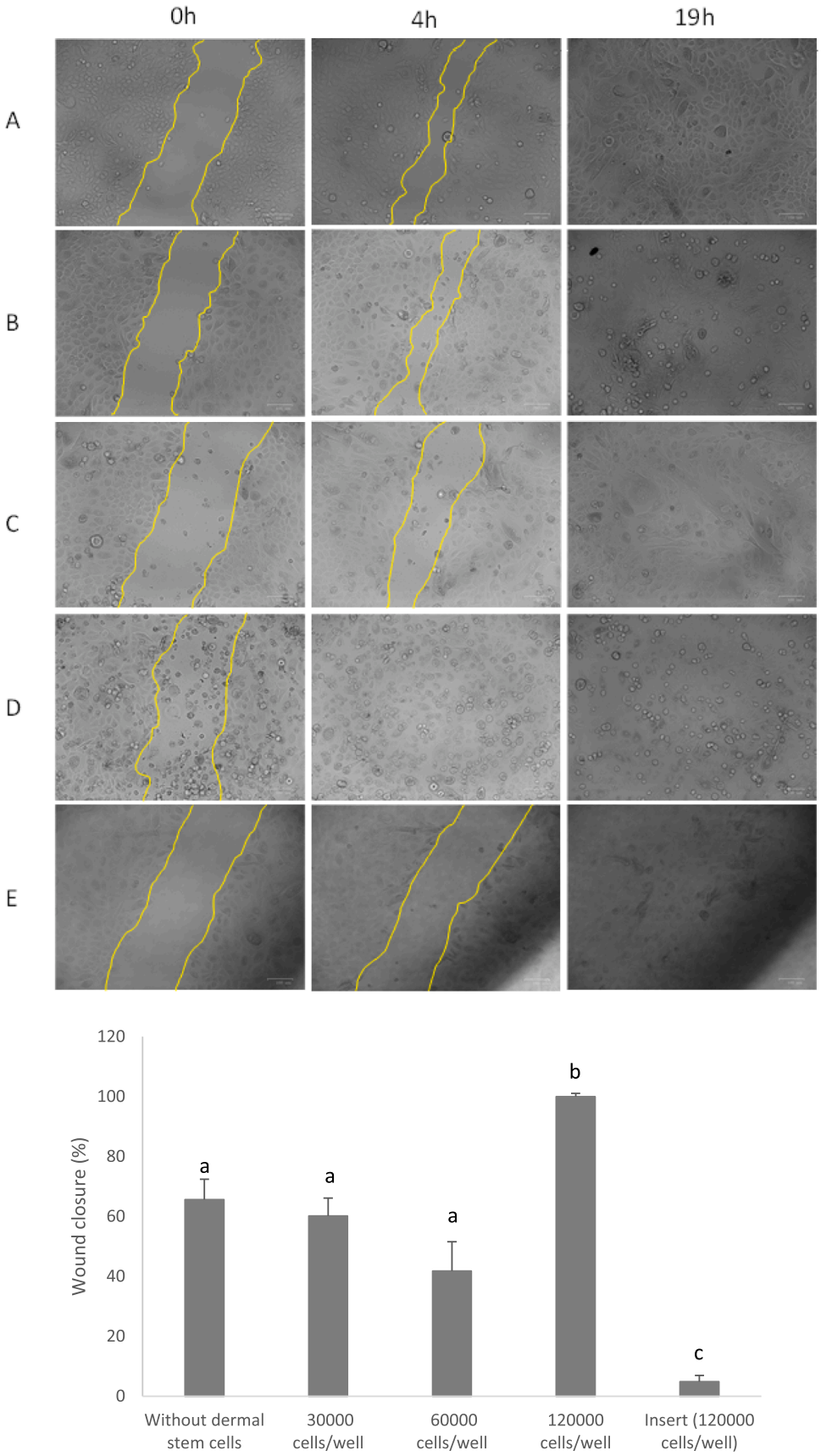

Fig. 18. Scratch assay. Confluent HEKa cells were scratch with a pipette tip in HYP20 (A), or with different concentrations of dermal stem cells 30,000 cells/well (B) 60,000 cells/well (C) and 120,000 cells/well (D on the well and E on an insert). The yellow lines indicate the limits of the wound area. At 19 h, all wounds were closed. The graph indicates the percentage of wound closure in the 5 conditions assayed (mean ± SEM). Different letters indicate statistical differences.

The conductivity of a hydrogel is generally due to the presence of ions in the medium and the electrical charges in the polymer chains of the hydrogel. The cell membrane is an instrumental component of the cells, and its structure is based on a lipid bilayer in which proteins are distributed, allowing the formation of channels for ion exchange. When cells are incorporated into a hydrogel, the cell membrane of the cells acts as a semi-permeable barrier, allowing ion exchange to take place, leading to change in conductivity. The conductivity values were lower after adding hMSC into the hydrogel. This fact is attributed to the membrane of the cells that acts as a semi-permeable barrier, allowing ion exchange to take place between the cytoplasm and the external environment of the cell (Cooper, 2000). Although the conductivity decreased when the cells were incorporated, high conductivity values were obtained which may contribute to enhance the cell-to-cell communication and cell adhesion and to induce the specific differentiation of hMSCs (Jin and Li, 2014; Soriano-Ruiz et al., 2019a).

We evaluated the bioadhesive properties of the hydrogel because, in wound healing, the hydrogel has to remain in contact with the wound to promote cell migration and cell proliferation. It is well known that dermal formulations can be easily removed from the skin due to factors such as humidity, temperature, and physical movement (Shaikh et al., 2011; Amorós-Galicia et al., 2022). It is therefore essential that the formulations exhibit bioadhesive properties for reepithelization of skin injuries. While it is true that skin wounds do not normally contain mucin, the goal of wound healing formulations is to adhere to and interact with the wound bed effectively. Porcine skin with intact stratum corneum can provide insight into how these formulations adhere to the surface of the skin. Although porcine skin may not perfectly mimic all aspects of human skin wounds (even though skin wounds might lack a stratum corneum), it offers valuable insights into the bioadhesive properties of wound healing formulations at the early stages of formulation development; it can be beneficial to assess bioadhesion in a controlled and consistent manner. Porcine skin with full stratum corneum provides this consistency and can serve as an initial screening tool and provide important preliminary data before moving on to more complex models. The bioadhesive capacity of the hydrogels was assessed by two different approaches: on one hand, the ex vivo approach in which the formulation was placed between two pieces of skin to determine the detachment force. On the other hand, the *in vitro* approach in which the bioadhesive properties of the formulation were evaluated based on the method used by García et al. (2017). The researchers assessed the bioadhesive capacity of wound dressing films incubating the films in a mucin solution and monitoring the changes in the zeta potential values. The poor bioadhesive property of poloxamer 407 hydrogels is a principal disadvantage of topical administration. The hydrogel, due to a rapid dissolution in contact with body fluids, led to short permanence on the place of application (Bellotti et al., 2023). The leakage test showed considerable distances in a short time compromising the correct dosage of the preparation, being insufficient to reach the internal cavities of the wound. Only the HYP20 hydrogel covered shorter a distance at 37 °C and pH = 5.5. Our results are in accordance with previous studies about hydrogels for vaginal application. Bellotti et al. (2023) developed a hydrophilic gel based on poloxamer 407 and xanthan gum and demonstrated that the hydrogels ran the longest distance, covering the entire slide length in few seconds.

The results of leakage are in line with bioadhesive strength because we obtained the highest bioadhesive force values at 37 °C for both formulations, possibly due to the fact that hydrogels have higher viscosity values at 37 than at 25 °C. The bioadhesive property was also evaluated measure the influence of the samples on the zeta potential of mucin. It was observed that the ζ value of the mucin solution became more positive when mixed it with the hydrogels. This change in value would be due to the interactions of the negative groups of mucin, such as carboxylate and sulfonate with the positive groups of the polymer of hydrogels (Gosecka and Gosecki, 2021). Polymer with bioadhesive properties is able neutralise mucin charge (Takeuchi et al., 2005). These results confirm de poor bioadhesive property of poloxamer 407 hydrogels. It should be noted that these methods are static and would not resemble the real conditions of application of the formulation, so *in vivo* studies would be necessary.

The extrudability properties of hydrogels are important to study in topical formulations. The highest extrudability values were obtained at 25 °C for both formulations, indicating that are require the maximum force to be extruded from the syringe. At 4 °C both hydrogels extrude more easily which can lead to spillage problems during application. It can be seen the addition of MSCs decreases the force to be applied for extrusion the hydrogel and consequently, extrudability values decrease. Therefore, the designed hydrogel provides a suitable niche for hMSCs in terms of application, as lower pressures and stress should be induced in hMSCs.

The spray angle of hydrogels decreased with increasing temperature due to gelation of the hydrogel. The different angles obtained could offer several advantages such as adaptation to different sizes of wounds, good coverage, adequate distribution of hMSC when applied.

The thermal behavior of fresh HYP20 hydrogel and freeze-dried HYP20 hydrogel was evaluated by TGA and DSC. The thermal degradation profiles of the hydrogels showed small differences related to the presence of the water. To the fresh HYP20 hydrogel, the first weight loss occurred between approximately at 30–140 °C, with a weight loss percentage of 79.95 %. This thermal degradation is mostly associated with the water loss of the polymeric hydrogel matrix. As reported in the literature, temperature ranges from 25 to 140 °C are associated with water loss in thermogravimetric analysis (Bala et al., 2000; Rocha et al., 2022) due to the water is the main component of hydrogel formulations. Thermal decomposition of albumin (56–69 °C) (Michnik, 2003) and sodium lactate (120–145 °C) (Ellis et al., 2003) presents in the hydrogel matrix also occurs in this temperature range. To the fresh HYP20 hydrogel a gradual loss of mass is observed in the temperature ranging from 140 to 322 °C. In this temperature range the thermal decomposition of the potassium chloride (approximately 300 °C) (Pan and Jiang, 2019) and calcium chloride (above 260 °C) (Fraissler et al., 2009) present in the medium takes place. The second major degradation event took place from 330 to 420 °C in both hydrogels and is associated with the polymer thermal decomposition, corroborating the previous results described by Pham et al. (2019) and (Rocha et al., 2022). At the end of the thermal curve of fresh HYP20 hydrogel and freeze-dried HYP20 hydrogel, was detected a loss weight of 0.28 mg in the temperature ranging from 420 to 756 °C and 0.74 mg from 420 to 870 °C, respectively. This thermal degradation is possibly associated with the sodium chloride of the polymeric hydrogel matrix (above 800 °C) (Klima et al., 2022).

The thermal study was completed by also performing a DSC analysis of the samples studied. In fresh HYP20 hydrogel the first endothermic peak was associated with the water loss. The second endothermic peak was corresponded to the degradation of polymer observed above, in the TGA. In contrast, in freeze-dried HYP20 hydrogel the first endothermic peak observed may correspond to phase change of the polymer and the second endothermic peak observed was also associated with the polymer degradation.

DSC has been used to detect and measure the temperature and heat involved in thermal events, such as micellization (Al Khateb et al., 2016; Boonlai et al., 2017). As can be seen in the plot, an endothermic peak was observed in the DSC thermogram at 15 °C which falls into the expected range similar to results obtained in previous studies (Antunes et al., 2011; Hirun et al., 2022). At low temperatures, poloxamer 407 chains are considered to exist in solution as non-associated entities. Polymer chain rearrangement can occur during heating, leading to micelle formation. The broad endothermic signal observed reflects the temperature and energy associated with this process. The critical micellization temperature is represented by the peak position of the endothermic signal. Heating caused partial disruption of the intermolecular interactions between water molecules and the hydrophobic

blocks of polymer, resulting in the assembly of dehydrated blocks and the transformation of monomers into micelles (Boonlai et al., 2017; Hirun et al., 2022).

The micelle size of the hydrogels was determined by dynamic light scattering using the Nano Zetasizer at different temperatures. The study showed an increase in size with increasing temperature from 4 to 37 °C for both formulations. Thus, no significant size differences were observed after incorporation of HMSCs. These results are due to the dehydration of the PEO chains after the temperature increase, resulting in the packing of more polymer chains into the micelle (Bodratti and Alexandridis, 2018).

The SEM images confirmed that poloxamer-based hydrogel possess high porosity and interconnected pores. The interconnected pores facilitate cell ingrowth, vascularization, and nutrient diffusion, which are essential for cell survival and enable the hydrogel to provide support for cell encapsulation. The average pore size of the hydrogel on tissue regeneration has been highlighted through experiments that demonstrate the optimum pore sizes for specific processes. For instance, a pore size of 5 μm is ideal for neovascularization, 5–15 μm for fibroblast ingrowth, and 20–125 μm for regeneration of adult mammalian skin (Annabi et al., 2010; Diniz et al., 2015).

Finally, it is well-known that certain polymeric solutions can undergo structural changes when they pass through a narrow conduit, due to the contraction or relaxation of polymeric chains, or compatibility differences between certain components (Abdellatif et al., 2020). The SEM images showed no change in the morphology of the hydrogels at the different temperatures tested.

Keratinocytes constitute the major cell type found in the epidermis. They play an essential role not only in maintaining the integrity of this barrier but also in the process of re-epithelialization process. During re-epithelialization, keratinocytes undergo migration, proliferation, and differentiation to effectively regenerate the epidermal barrier (Jiang et al., 2020; Piipponen et al., 2020).

The addition of the different concentrations of HYP20-C hydrogel to the epithelium did not affect the viability of keratinocytes or their capacity of healing as all the conditions assayed were able to close the wound area at 19 h. In a shorter period of time (4 h), the highest proportion assayed (with 10 times more hMSCs than keratinocytes) was able to completely reduce the wound area, which was earlier than in the other conditions assayed with or without hMSCs. Interestingly, when the HYP20-C hydrogel at the highest concentration were added to an insert instead of directly into the well to better observe the wound area, thus hMSCs were not in contact with the keratinocytes, the reduction of the wound was minimal suggesting that the healing properties of the hMSCs is not due to the metabolites released to the medium but to the direct interaction with the keratinocytes. Furthermore, at 19 h the wound area of the epithelium above the insert was also closed reinforcing the idea that the HYP20-C hydrogel applied directly is a better option to accelerate the process of closure.

These results confirmed that the developed hydrogel has a potential use in would healing to superficial skin injures. However, it would be interesting to assay this hydrogel *in vivo* to check its efficacy on skin which is a more complex structure with different properties and cell types involved.

5. Conclusions

A hydrogel loaded with hMSCs was developed for its use in the treatment of skin superficial wound. From a physicochemical perspective, HYP20-C had an optimal swelling property, degradation rate, porosity, surface properties, spreadability and extrudability. It also exhibited the required rheological properties necessary for its use as in situ gel systems for topical administration. Furthermore, hydrogel showed hydrophilic properties that play a crucial role in preventing bacterial infections, promoting cell migration, and preventing the loss of body fluids and essential nutrients *in vivo*. The HYP20-C provided a good environment for cell viability. In addition, the wound healing assay indicated that the HYP20-C did not cause any damage to the cell layer and showed complete restoration of keratinocyte presence at the wound site in a shorter period of time. Based on all results discussed above we demonstrated that HYP20-C is a suitable formulation for its use in tissue engineering and can be proposed as a potential candidate for superficial wound healing.

Funding

This work was supported by the Ministerio de Economía, Industria y Competitividad (FEDER funds, project RTC-2016-5451-1), AdvanceCat with the support of ACCIÓ (Catalonia Trade & Investment; Generalitat de Catalunya) under the Catalonian European Regional Development Fund operational program, 2014–2020 (to PG-M), FCT—Fundação para a Ciência e a Tecnologia, I.P., in the scope of the project UIDP/04378/2020 and UIDB/04378/2020 of the Research Unit on Applied Molecular Biosciences—UCIBIO and the project LA/P/0140/2020 of the Associate Laboratory Institute for Health and Bioeconomy—i4HB.

Declaration of Competing Interest

The authors declare that they have no known competing financial interests or personal relationships that could have appeared to influence the work reported in this paper.

Data availability

Data will be made available on request.

Acknowledgements

We thank the TEM-SEM Electron Microscopy Unit from Scientific and Technological Centers (CCiTUB), Universitat de Barcelona, and its staff for their support and advice on SEM technique.

Ethics approval

Ethics approval was obtained from the Ethics Committee of the University of Barcelona, Spain (CEEA-UB) code 10617 for the animal experimentation using pig skin. Animals were sacrificed under veterinary supervision at the Animal Facility of the Bellvitge Campus of the University of Barcelona (Spain). Ethics approval was obtained from the Ethics Committee of the of Clinical University Hospital of Málaga, Spain, for the collection of hMSCs from infrapatellar fat pad of patients with osteoarthritis (OA) during joint replacement surgery. Fat tissue was collected after informed consent from all patients and approval from the Ethics Committee.

Authors contribution

All authors have actively contributed to the conception and design of the study, data acquisition, analysis and interpretation, drafting the article and revising it critically for important intellectual content, and have approved the final version to be submitted.

References

Abdellatif, M.M., Khalil, I.A., Elakkad, Y.E., Eliwa, H.A., Samir, T.M., Al-Mokaddem, A. K., 2020. Formulation and characterization of sertaconazole nitrate mucoadhesive liposomes for vaginal candidiasis. Int. J. Nanomed. 15, 4079–4090.

Al Khateb, K., Ozhmukhametova, E.K., Mussin, M.N., Seilkhanov, S.K., Rakhypbekov, T. K., Lau, W.M., Khutoryanskiy, V.V., 2016. In situ gelling systems based on Pluronic F127/Pluronic F68 formulations for ocular drug delivery. Int. J. Pharm. 502, 70–79.

Alvarado-Gomez, E., Martínez-Castañon, G., Sanchez-Sanchez, R., Ganem-Rondero, A., Yacaman, M.J., Martinez-Gutierrez, F., 2018. Evaluation of anti-biofilm and cytotoxic effect of a gel formulation with Pluronic F-127 and silver nanoparticles as a

potential treatment for skin wounds. Mater. Sci. Eng. C, Mater. Biol. Appl. 92, 621–630.
Amores, S., Domenech, J., Colom, H., Calpena, A.C., Clares, B., Gimeno, Á., Lauroba, J., 2014. An improved cryopreservation method for porcine buccal mucosa in ex vivo drug permeation studies using Franz diffusion cells. Eur. J. Pharm. Sci. 60, 49–54.
Amorós-Galicia, L., Nardi-Ricart, A., Verdugo-González, C., Arroyo-García, C.M., García-Montoya, E., Pérez-Lozano, P., Suñé-Negre, J.M., Suñé-Pou, M., 2022. Development of a standardized method for measuring bioadhesion and mucoadhesion that is applicable to various pharmaceutical dosage forms. Pharmaceutics 14.
Annabi, N., Nichol, J.W., Zhong, X., Ji, C., Koshy, S., Khademhosseini, A., Dehghani, F., 2010. Controlling the porosity and microarchitecture of hydrogels for tissue engineering. Tissue Eng. Part B, Rev. 16, 371–383.
Antunes, F.E., Gentile, L., Rossi, C.O., Tavano, L., Ranieri, G.A., 2011. Gels of Pluronic F127 and nonionic surfactants from rheological characterization to controlled drug permeation. Colloids Surf. B, Biointerfaces 87, 42–48.
Arévalo-Silva, C.A., Eavey, R.D., Cao, Y., Vacanti, M., Weng, Y., Vacanti, C.A., 2000. Internal support of tissue-engineered cartilage. Arch. Otolaryngol.–Head & Neck Surg. 126, 1448–1452.
Augustine, R., Hasan, A., Yadu Nath, V.K., Thomas, J., Augustine, A., Kalarikkal, N., Moustafa, A.-E.-A., Thomas, S., 2018. Electrospun polyvinyl alcohol membranes incorporated with green synthesized silver nanoparticles for wound dressing applications. J. Mater. Sci. - Mater. Med. 29, 163.
Bala, P., Samantaray, B.K., Srivastava, S.K., 2000. Dehydration transformation in Ca-montmorillonite. Bull. Mater. Sci. 23, 61–67.
Baloglu, E., Karavana, S.Y., Senyigit, Z.A., Guneri, T., 2011. Rheological and mechanical properties of poloxamer mixtures as a mucoadhesive gel base. Pharm. Dev. Technol. 16, 627–636.
Batista, C.M., de Queiroz, L.A., Alves, Â.V.F., Reis, E.C.A., Santos, F.A., Castro, T.N., Lima, B.S., Araújo, A.A.S., Godoy, C.A.P., Severino, P., Cano, A., Santini, A., Capasso, R., de Albuquerque Júnior, R.L.C., Cardoso, J.C., Souto, E.B., 2022. Photoprotection and skin irritation effect of hydrogels containing hydroalcoholic extract of red propolis: a natural pathway against skin cancer. Heliyon 8, e08893.
Bayani, J., Squire, J.A., 2004. Traditional banding of chromosomes for cytogenetic analysis. In: Current Protocols in Cell Biology, Chapter 22, Unit 22.23.
Bellotti, D., D'Accolti, M., Pula, W., Huang, N., Simeliere, F., Caselli, E., Esposito, E., Remelli, M., 2023. Calcitermin-loaded smart gels activity against *Candida albicans*: a preliminary in vitro study. Gels (Basel, Switzerland) 9.
Bian, D., Wu, Y., Song, G., Azizi, R., Zamani, A., 2022. The application of mesenchymal stromal cells (MSCs) and their derivative exosome in skin wound healing: a comprehensive review. Stem Cell Res. Ther. 13, 24.
Bodratti, A.M., Alexandridis, P., 2018. Formulation of poloxamers for drug delivery. J. Funct. Biomater. 9.
Boonlai, W., Tantishaiyakul, V., Hirun, N., Phaisan, S., Uma, T., 2017. The effect of the preservative methylparaben on the thermoresponsive gelation behavior of aqueous solutions of poloxamer 407. J. Mol. Liq. 240, 622–629.
Brugués, A.P., Naveros, B.C., Calpena Campmany, A.C., Pastor, P.H., Saladrigas, R.F., Lizandra, C.R., 2015. Developing cutaneous applications of paromomycin entrapped in stimuli-sensitive block copolymer nanogel dispersions. Nanomedicine (Lond.) 10, 227–240.
Cao, Y., Rodriguez, A., Vacanti, M., Ibarra, C., Arevalo, C., Vacanti, C.A., 1998. Comparative study of the use of poly(glycolic acid), calcium alginate and pluronics in the engineering of autologous porcine cartilage. J. Biomater. Sci. Polym. Ed. 9, 475–487.
Cardin, A.D., Weintraub, H.J., 1989. Molecular modeling of protein-glycosaminoglycan interactions. Arteriosclerosis (Dallas, Tex.) 9, 21–32.
Ceccaldi, C., Assaad, E., Hui, E., Buccionyte, M., Adoungotchodo, A., Lerouge, S., 2017. Optimization of injectable thermosensitive scaffolds with enhanced mechanical properties for cell therapy. Macromol. Biosci. 17.
Chen, Y.-M., Yang, J.-J., Osada, Y., Gong, J.P., 2011. Synthetic hydrogels as scaffolds for manipulating endothelium cell behaviors. Chin. J. Polym. Sci. 29, 23–41.
Ci, L., Huang, Z., Liu, Y., Liu, Z., Wei, G., Lu, W., 2017. Amino-functionalized poloxamer 407 with both mucoadhesive and thermosensitive properties: preparation, characterization and application in a vaginal drug delivery system. Acta Pharm. Sin. B 7, 593–602.
Contreras, M.D., Sanchez, R., 2002. Application of a factorial design to the study of the flow behavior, spreadability and transparency of a Carbopol ETD 2020 gel. Part II. Int. J. Pharm. 234, 149–157.
Cooper, G.M., 2000. The cell: a molecular approach, in: Transport of Small Molecules, second edition, Sinauer Associates, Sunderland, MA, 2000, Available from: https://www.ncbi.nlm.nih.gov/books/NBK9847/.
Da, L.C., Huang, Y.Z., Xie, H.Q., 2017. Progress in development of bioderived materials for dermal wound healing. Regener. Biomater. 4, 325–334.
de Almeida, B.M., Dos Santos, I.D.D., de Carvalho, F.M.A., Correa, L.C., Cunha, J.L.S., Dariva, C., Severino, P., Cardoso, J.C., Souto, E.B., de Albuquerque-Junior, R.L.C., 2022. *Himatanthus bracteatus*-composed in situ polymerizable hydrogel for wound healing. Int. J. Mol. Sci. 23.
de Castro, K.C., Coco, J.C., Dos Santos, E.M., Ataide, J.A., Martinez, R.M., do Nascimento, M.H.M., Prata, J., da Fonte, P., Severino, P., Mazzola, P.G., Baby, A.R., Souto, E.B., de Araujo, D.R., Lopes, A.M., 2023. Pluronic(R) triblock copolymer-based nanoformulations for cancer therapy: a 10-year overview. J. Control. Release 353, 802–822.
DiBartola, S.P., 2012. Chapter 3 - disorders of sodium and water: hypernatremia and hyponatremia. In: DiBartola, S.P. (Ed.), Fluid, Electrolyte, and Acid-Base Disorders in Small Animal Practice, fourth edition. W.B. Saunders, Saint Louis, pp. 45–79.
Diniz, I.M., Chen, C., Xu, X., Ansari, S., Zadeh, H.H., Marques, M.M., Shi, S., Moshaverinia, A., 2015. Pluronic F-127 hydrogel as a promising scaffold for encapsulation of dental-derived mesenchymal stem cells. J. Mater. Sci. - Mater. Med. 26, 153.
do Nascimento, M.F., de Oliveira, C.R., Cardoso, J.C., Bordignon, N.C.T., Gondak, R., Severino, P., Souto, E.B., de Albuquerque Junior, R.L.C., 2023. UV-polymerizable methacrylated gelatin (GelMA)-based hydrogel containing tannic acids for wound healing. Drug Deliv. Transl. Res.
Dong, Z., Zhang, Q., Wang, C., Hu, W., Yu, X., Guo, M., Zhang, X., Sun, M., Du, S., Lu, Y., 2023. Combined thermosensitive gel co-loaded with dermaseptin-PP and PTX liposomes for effective local chemotherapy. Int. J. Nanomed. 18, 413–424.
Dumortier, G., Grossiord, J.L., Agnely, F., Chaumeil, J.C., 2006. A review of poloxamer 407 pharmaceutical and pharmacological characteristics. Pharm. Res. 23, 2709–2728.
El Moussaoui, S., Fernández-Campos, F., Alonso, C., Limón, D., Halbaut, L., Garduño-Ramirez, M.L., Calpena, A.C., Mallandrich, M., 2021. Topical mucoadhesive alginate-based hydrogel loading ketorolac for pain management after pharmacotherapy, ablation, or surgical removal in condyloma acuminata. Gels (Basel, Switzerland) 7.
Ellis, A.V., Kannangara, G.S.K., Wilson, M.A., 2003. Chemistry of sodium lactate formation under simulated alumina refinery conditions. Ind. Eng. Chem. Res. 42, 3185–3189.
Escobar-Chávez, J.J., López-Cervantes, M., Naïk, A., Kalia, Y.N., Quintanar-Guerrero, D., Ganem-Quintanar, A., 2006. Applications of thermo-reversible pluronic F-127 gels in pharmaceutical formulations. J. Pharm. Pharm. Sci.: Publ. Can. Soc. Pharm. Sci. Societe canadienne des sciences pharmaceutiques 9, 339–358.
Esposito, E., Drechsler, M., Huang, N., Pavoni, G., Cortesi, R., Santonocito, D., Puglia, C., 2016. Ethosomes and organogels for cutaneous administration of crocin. Biomed. Microdevices 18, 108.
Fakhari, A., Corcoran, M., Schwarz, A., 2017. Thermogelling properties of purified poloxamer 407. Heliyon 3, e00390.
FDA, 2023. Food and Drug Administration, Inactive Ingredient Search for Approved Drug Products. https://www.accessdata.fda.gov/scripts/cder/iig/index.cfm (accessed on 23rd August 2023).
Fedorovich, N.E., Swennen, I., Girones, J., Moroni, L., van Blitterswijk, C.A., Schacht, E., Alblas, J., Dhert, W.J., 2009. Evaluation of photocrosslinked Lutrol hydrogel for tissue printing applications. Biomacromolecules 10, 1689–1696.
Flégeau, K., Pace, R., Gautier, H., Rethore, G., Guicheux, J., Le Visage, C., Weiss, P., 2017. Toward the development of biomimetic injectable and macroporous biohydrogels for regenerative medicine. Adv. Colloid Interface Sci. 247, 589–609.
Fraissler, G., Jöller, M., Brunner, T., Obernberger, I., 2009. Influence of dry and humid gaseous atmosphere on the thermal decomposition of calcium chloride and its impact on the remove of heavy metals by chlorination. Chem. Eng. Process. 48, 380–388.
Fu, M., Liang, Y., Lv, X., Li, C., Yang, Y.Y., Yuan, P., Ding, X., 2021. Recent advances in hydrogel-based anti-infective coatings. J. Mater. Sci. Technol. 85, 169–183.
Gálvez-Martín, P., Hmadcha, A., Soria, B., Calpena-Campmany, A.C., Clares-Naveros, B., 2014. Study of the stability of packaging and storage conditions of human mesenchymal stem cell for intra-arterial clinical application in patient with critical limb ischemia. Eur. J. Pharm. Biopharm.: Off. J. Arbeitsgemeinschaft fur Pharmazeutische Verfahrenstechnik e.V 86, 459–468.
García, M.C., Aldana, A.A., Tártara, L.I., Alovero, F., Strumia, M.C., Manzo, R.H., Martinelli, M., Jimenez-Kairuz, A.F., 2017. Bioadhesive and biocompatible films as wound dressing materials based on a novel dendronized chitosan loaded with ciprofloxacin. Carbohydr. Polym. 175, 75–86.
Giuliano, E., Paolino, D., Cristiano, M.C., Fresta, M., Cosco, D., 2020. Rutin-Loaded Poloxamer 407-Based hydrogels for in situ administration: stability profiles and rheological properties. Nanomaterials (Basel) 10.
Giuliano, E., Paolino, D., Fresta, M., Cosco, D., 2018. Mucosal applications of Poloxamer 407-based hydrogels: an overview. Pharmaceutics 10.
Gonzalez Garcia, J.R., Meza-Espinoza, J.P., 2006. Use of the international system for human cytogenetic nomenclature (ISCN). Blood 108, 3952–3953 author reply 3953.
Gosecka, M., Gosecki, M., 2021. Antimicrobial polymer-based hydrogels for the intravaginal therapies-engineering considerations. Pharmaceutics 13.
Guadix, J.A., López-Beas, J., Clares, B., Soriano-Ruiz, J.L., Zugaza, J.L., Gálvez-Martín, P., 2019. Principal criteria for evaluating the quality, safety and efficacy of hMSC-based products in clinical practice: current approaches and challenges. Pharmaceutics 11.
Guillamat-Prats, R., 2021. The role of MSC in wound healing, scarring and regeneration. Cells 10.
Han, G., Ceilley, R., 2017. Chronic wound healing: a review of current management and treatments. Adv. Ther. 34, 599–610.
Hirun, N., Kraisit, P., Tantishaiyakul, V., 2022. Thermosensitive polymer blend composed of Poloxamer 407, Poloxamer 188 and polycarbophil for the use as mucoadhesive in situ gel. Polymers 14.
Ho, T.C., Chang, C.C., Chan, H.P., Chung, T.W., Shu, C.W., Chuang, K.P., Duh, T.H., Yang, M.H., Tyan, Y.C., 2022. Hydrogels: properties and applications in biomedicine. Molecules 27.
Hu, M.S., Borrelli, M.R., Lorenz, H.P., Longaker, M.T., Wan, D.C., 2018. Mesenchymal stromal cells and cutaneous wound healing: a comprehensive review of the background, role, and therapeutic potential. Stem Cells Int. 2018, 6901983.
Huang, C., Dong, L., Zhao, B., Lu, Y., Huang, S., Yuan, Z., Luo, G., Xu, Y., Qian, W., 2022. Anti-inflammatory hydrogel dressings and skin wound healing. Clin. Transl. Med. 12, e1094.
Jaramillo, V., Díaz, E., Muñoz, L.N., González-Barrios, A.F., Rodríguez-Cortina, J., Cruz, J.C., Muñoz-Camargo, C., 2023. Enhancing wound healing: a novel topical emulsion combining CW49 peptide and lavender essential oil for accelerated regeneration and antibacterial protection. 15, 1739.

Jiang, Y., Tsoi, L.C., Billi, A.C., Ward, N.L., Harms, P.W., Zeng, C., Maverakis, E., Kahlenberg, J.M., Gudjonsson, J.E., 2020. Cytokinocytes: the diverse contribution of keratinocytes to immune responses in skin. JCI Insight 5.
Jin, G., Li, K., 2014. The electrically conductive scaffold as the skeleton of stem cell niche in regenerative medicine. Mater. Sci. Eng. C, Mater. Biol. Appl. 45, 671–681.
Johnston, T.P., Punjabi, M.A., Froelich, C.J., 1992. Sustained Delivery of Interleukin-2 from a Poloxamer 407 gel matrix following intraperitoneal injection in mice. Pharm. Res. 9, 425–434.
Kaisang, L., Siyu, W., Lijun, F., Daoyan, P., Xian, C.J., Jie, S., 2017. Adipose-derived stem cells seeded in Pluronic F-127 hydrogel promotes diabetic wound healing. J. Surg. Res. 217, 63–74.
Khattak, S.F., Bhatia, S.R., Roberts, S.C., 2005. Pluronic F127 as a cell encapsulation material: utilization of membrane-stabilizing agents. Tissue Eng. 11, 974–983.
Kim, D.K., Sim, B.R., Khang, G., 2016. Nature-derived aloe vera gel blended silk fibroin film scaffolds for cornea endothelial cell regeneration and transplantation. ACS Appl. Mater. Interfaces 8, 15160–15168.
Klima, K.M., Schollbach, K., Brouwers, H.J.H., Yu, Q., 2022. Enhancing the thermal performance of Class F fly ash-based geopolymer by sodalite. Constr. Build. Mater. 314, 125574.
Lee, C.H., Moturi, V., Lee, Y., 2009. Thixotropic property in pharmaceutical formulations. J. Control. Release 136, 88–98.
Lenaerts, V., Triqueneaux, C., Quartern, M., Rieg-Falson, F., Couvreur, P., 1987. Temperature-dependent rheological behavior of Pluronic F-127 aqueous solutions. Int. J. Pharm. 39, 121–127.
Li, L., Yu, F., Zheng, L., Wang, R., Yan, W., Wang, Z., Xu, J., Wu, J., Shi, D., Zhu, L., Wang, X., Jiang, Q., 2019. Natural hydrogels for cartilage regeneration: modification, preparation and application. J. Orthopaed. Transl. 17, 26–41.
Li, W.Z., Zhao, N., Zhou, Y.Q., Yang, L.B., Xiao-Ning, W., Bao-Hua, H., Peng, K., Chun-Feng, Z., 2012. Post-expansile hydrogel foam aerosol of PG-liposomes: a novel delivery system for vaginal drug delivery applications. Eur. J. Pharm. Sci. 47, 162–169.
Liang, Y., He, J., Guo, B., 2021. Functional hydrogels as wound dressing to enhance wound healing. ACS Nano 15, 12687–12722.
Linse, P., 1993. Micellization of poly(ethylene oxide)-poly(propylene oxide) block copolymers in aqueous solution. Macromolecules 26, 4437–4449.
Liu, Y., Fu, S., Lin, L., Cao, Y., Xie, X., Yu, H., Chen, M., Li, H., 2017a. Redox-sensitive Pluronic F127-tocopherol micelles: synthesis, characterization, and cytotoxicity evaluation. Int. J. Nanomed. 12, 2635–2644.
Liu, Y., Yang, F., Feng, L., Yang, L., Chen, L., Wei, G., Lu, W., 2017b. In vivo retention of poloxamer-based in situ hydrogels for vaginal application in mouse and rat models. Acta Pharm. Sin. B 7, 502–509.
Mallandrich, M., Fernández-Campos, F., Clares, B., Halbaut, L., Alonso, C., Coderch, L., Garduño-Ramírez, M.L., Andrade, B., Del Pozo, A., Lane, M.E., Calpena, A.C., 2017. Developing transdermal applications of ketorolac tromethamine entrapped in stimuli sensitive block copolymer hydrogels. Pharm. Res. 34, 1728–1740.
Matthew, J.E., Nazario, Y.L., Roberts, S.C., Bhatia, S.R., 2002. Effect of mammalian cell culture medium on the gelation properties of Pluronic F127. Biomaterials 23, 4615–4619.
Mei, L., Chen, J., Yu, S., Huang, Y., Xie, Y., Wang, H., Pan, X., Wu, C., 2017. Expansible thermal gelling foam aerosol for vaginal drug delivery. Drug Deliv. 24, 1325–1337.
Mendes, A.C., Sevilla Moreno, J., Hanif, M., Chen, M., Chronakis, I.S., 2018. Morphological, mechanical and mucoadhesive properties of electrospun chitosan/phospholipid hybrid nanofibers. Int. J. Mol. Sci. 19.
Michnik, A., 2003. Thermal stability of bovine serum albumin DSC study. J. Therm. Anal. Calorim. 71, 509–519.
Naskar, A., Kim, K.S., 2020. Recent advances in nanomaterial-based wound-healing therapeutics. Pharmaceutics 12.
Nurzynska, A., Klimek, K., Palka, K., Szajnecki, Ł., Ginalska, G., 2021. Curdlan-based hydrogels for potential application as dressings for promotion of skin wound healing-preliminary in vitro studies. Materials (Basel, Switzerland) 14.
Nuttelman, C.R., Tripodi, M.C., Anseth, K.S., 2005. Synthetic hydrogel niches that promote hMSC viability. Matrix Biol.: J. Int. Soc. Matrix Biol. 24, 208–218.
Oshiro, A., da Silva, D.C., de Mello, J.C., de Moraes, V.W., Cavalcanti, L.P., Franco, M.K., Alkschbirs, M.I., Fraceto, L.F., Yokaichiya, F., Rodrigues, T., de Araujo, D.R., 2014. Pluronics f-127/l-81 binary hydrogels as drug-delivery systems: influence of physicochemical aspects on release kinetics and cytotoxicity. Langmuir: ACS J. Surf. Colloids 30, 13689–13698.
Pan, L., Jiang, Y., 2019. Evaluating the effects of KCl on thermal behavior and reaction kinetics of medium density fiberboard pyrolysis. Materials (Basel, Switzerland) 12.
Pan, J.F., Liu, N.H., Sun, H., Xu, F., 2014. Preparation and characterization of electrospun PLCL/Poloxamer nanofibers and dextran/gelatin hydrogels for skin tissue engineering. PLoS One 9, e112885.
Parvanian, S., Zha, H., Su, D., Xi, L., Jiu, Y., Chen, H., Eriksson, J.E., Cheng, F., 2021. Exosomal vimentin from adipocyte progenitors protects fibroblasts against osmotic stress and inhibits apoptosis to enhance wound healing. Int. J. Mol. Sci. 22.
Perez-Valle, A., Del Amo, C., Andia, I., 2020. Overview of current advances in extrusion bioprinting for skin applications. Int. J. Mol. Sci. 21.
Pham, L., Dang, L.H., Truong, M.D., Nguyen, T.H., Le, L., Le, V.T., Nam, N.D., Bach, L.G., Nguyen, V.T., Tran, N.Q., 2019. A dual synergistic of curcumin and gelatin on thermal-responsive hydrogel based on Chitosan-P123 in wound healing application. Biomed. Pharmacother. 117, 109183.
Piipponen, M., Li, D., Landén, N.X., 2020. The immune functions of keratinocytes in skin wound healing. Int. J. Mol. Sci. 21.
Pironi, A.M., Melero, A., Eloy, J.O., Guillot, A.J., Pini Santos, K., Chorilli, M., 2022. Solid dipersions included in poloxamer hydrogels have favorable rheological properties for topical application and enhance the in vivo antiinflammatory effect of ursolic acid. J. Drug Delivery Sci. Technol. 74, 103602.
Pretel, E., Arias, J.L., Cabeza, L., Melguizo, C., Prados, J., Mallandrich, M., Suñer, J., Clares, B., 2017. Development of biomedical 5-fluorouracil nanoplatforms for colon cancer chemotherapy: Influence of process and formulation parameters. Int. J. Pharm. 530, 155–164.
Qian, Z., Wang, H., Bai, Y., Wang, Y., Tao, L., Wei, Y., Fan, Y., Guo, X., Liu, H., 2020. Improving chronic diabetic wound healing through an injectable and self-healing hydrogel with platelet-rich plasma release. ACS Appl. Mater. Interfaces 12, 55659–55674.
Qing, X., He, G., Liu, Z., Yin, Y., Cai, W., Fan, L., Fardim, P., 2021. Preparation and properties of polyvinyl alcohol/N–succinyl chitosan/lincomycin composite antibacterial hydrogels for wound dressing. Carbohydr. Polym. 261, 117875.
Ramos, P., 2022. Application of thermal analysis to evaluate pharmaceutical preparations containing theophylline. 15, 1268.
Rocha, M.S., Batista, J.V.C., Melo, M.N.O., Campos, V.E.B.d., Toledo, A.L.M.M., Oliveira, A.P., Picciani, P.H.S., Baumgartner, S., Holandino, C., 2022. Pluronic® F127 Thermoresponsive Viscum album hydrogel: physicochemical features and cellular in vitro evaluation. 14, 2775.
Rodrigues, C., de Assis, A.M., Moura, D.J., Halmenschlager, G., Saffi, J., Xavier, L.L., Fernandes Mda, C., Wink, M.R., 2014. New therapy of skin repair combining adipose-derived mesenchymal stem cells with sodium carboxymethylcellulose scaffold in a pre-clinical rat model. PLoS One 9, e96241.
Semak, V., Semakova, J., Halbaut, L., Aso, E., Ferrer, I., Calpena, A., Escolano, C., Perales, J.C., 2012. Synthesis of triheptanoin and formulation as a solid diet for rodents. 114, 889–895.
Shachaf, Y., Gonen-Wadmany, M., Seliktar, D., 2010. The biocompatibility of PluronicF127 fibrinogen-based hydrogels. Biomaterials 31, 2836–2847.
Shaikh, R., Raj Singh, T.R., Garland, M.J., Woolfson, A.D., Donnelly, R.F., 2011. Mucoadhesive drug delivery systems. J. Pharm. Bioallied Sci. 3, 89–100.
Shin, S.M., Baek, E.J., Kim, K.H., Kim, K.J., Park, E.J., 2023. Polydeoxyribonucleotide exerts opposing effects on ERK activity in human skin keratinocytes and fibroblasts. Mol. Med. Rep. 28.
Sivaraj, D., Chen, K., Chattopadhyay, A., Henn, D., Wu, W., Noishiki, C., Magbual, N.J., Mittal, S., Mermin-Bunnell, A.M., Bonham, C.A., Trotsyuk, A.A., Barrera, J.A., Padmanabhan, J., Januszyk, M., Gurtner, G.C., 2021. Hydrogel scaffolds to deliver cell therapies for wound healing. Front. Bioeng. Biotechnol. 9, 660145.
Soriano-Ruiz, J.L., Gálvez-Martín, P., López-Ruiz, E., Suñer-Carbó, J., Calpena-Campmany, A.C., Marchal, J.A., Clares-Naveros, B., 2019a. Design and evaluation of mesenchymal stem cells seeded chitosan/glycosaminoglycans quaternary hydrogel scaffolds for wound healing applications. Int. J. Pharm. 570, 118632.
Soriano-Ruiz, J.L., Suñer-Carbó, J., Calpena-Campmany, A.C., Bozal-de Febrer, N., Halbaut-Bellowa, L., Boix-Montañés, A., Souto, E.B., Clares-Naveros, B., 2019b. Clotrimazole multiple W/O/W emulsion as anticandidal agent: characterization and evaluation on skin and mucosae. Colloids Surf. B: Biointerfaces 175, 166–174.
Soriano-Ruiz, J.L., Calpena-Campmany, A.C., Silva-Abreu, M., Halbout-Bellowa, L., Bozal-de Febrer, N., Rodríguez-Lagunas, M.J., Clares-Naveros, B., 2020. Design and evaluation of a multifunctional thermosensitive poloxamer-chitosan-hyaluronic acid gel for the treatment of skin burns. Int. J. Biol. Macromol. 142, 412–422.
Stan, D., Tanase, C., Avram, M., Apetrei, R., Mincu, N.B., Mateescu, A.L., Stan, D., 2021. Wound healing applications of creams and "smart" hydrogels. Exp. Dermatol. 30, 1218–1232.
Stupack, D.G., Cheresh, D.A., 2002. Get a ligand, get a life: integrins, signaling and cell survival. J. Cell Sci. 115, 3729–3738.
Szulc-Musioł, B., Dolińska, B., Kołodziejska, J., Ryszka, F., 2017. Influence of plasma on the physical properties of ointments with quercetin. Acta Pharm. (Zagreb, Croatia) 67, 569–578.
Takeuchi, H., Thongborisute, J., Matsui, Y., Sugihara, H., Yamamoto, H., Kawashima, Y., 2005. Novel mucoadhesion tests for polymers and polymer-coated particles to design optimal mucoadhesive drug delivery systems. Adv. Drug Deliv. Rev. 57, 1583–1594.
Tripathi, A., Melo, J.S., 2015. Preparation of a sponge-like biocomposite agarose–chitosan scaffold with primary hepatocytes for establishing an in vitro 3D liver tissue model. RSC Adv. 5, 30701–30710.
Umar, A.K., Butarbutar, M., Sriwidodo, S., Wathoni, N., 2020. Film-forming sprays for topical drug delivery. Drug Des. Devel. Ther. 14, 2909–2925.
Wiegand, C., Hipler, U.C., Elsner, P., Tittelbach, J., 2021. Keratinocyte and fibroblast wound healing in vitro is repressed by non-optimal conditions but the reparative potential can be improved by water-filtered infrared A. Biomedicines 9.
Xu, N., Xu, J., Zheng, X., Hui, J., 2020. Preparation of injectable composite hydrogels by blending poloxamers with calcium carbonate-crosslinked sodium alginate. ChemistryOpen 9, 451–458.
Yang, T.T., Cheng, Y.Z., Qin, M., Wang, Y.H., Yu, H.L., Wang, A.L., Zhang, W.F., 2017. Thermosensitive chitosan hydrogels containing polymeric microspheres for vaginal drug delivery. Biomed Res. Int. 2017, 3564060.
Yu, N., Li, T., Qiu, Z., Xu, J., Li, Y., Huang, J., Yang, Y., Li, Z., Long, X., Zhang, H., 2023. Wip1 regulates wound healing by affecting activities of keratinocytes and endothelial cells through ATM-p53 and mTOR signaling. Burns: J. Int. Soc. Burn Injuries.
Yuan, Y., Lee, T.R., 2013. Contact angle and wetting properties. In: Bracco, G., Holst, B. (Eds.), Surface science techniques, Springer Series in Surface Sciences (SSSUR), Springer Berlin, Heidelberg, pp. 3–34, doi: 10.1007/978-3-642-34243-1_1.
ZetaSizer, 2023. https://www.cif.iastate.edu/sites/default/files/uploads/Other_Inst/Particle %20Size/Zetasizer %20Nano %20ZS %20User %20Manual.pdf (accessed on 11th October 2023).
Zhao, F., Cheng, J., Zhang, J., Yu, H., Dai, W., Yan, W., Sun, M., Ding, G., Li, Q., Meng, Q., Liu, Q., Duan, X., Hu, X., Ao, Y., 2021. Comparison of three different acidic

solutions in tendon decellularized extracellular matrix bio-ink fabrication for 3D cell printing. Acta Biomater. 131, 262–275.
Zhao, X., Irvine, S.A., Agrawal, A., Cao, Y., Lim, P.Q., Tan, S.Y., Venkatraman, S.S., 2015. 3D patterned substrates for bioartificial blood vessels – the effect of hydrogels on aligned cells on a biomaterial surface. Acta Biomater. 26, 159–168.
Zielińska, A., Eder, P., Rannier, L., Cardoso, J.C., Severino, P., Silva, A.M., Souto, E.B., 2022. Hydrogels for modified-release drug delivery systems. Curr. Pharm. Des. 28, 609–618.
Zielinska, A., Karczewski, J., Eder, P., Kolanowski, T., Szalata, M., Wielgus, K., Szalata, M., Kim, D., Shin, S.R., Slomski, R., Souto, E.B., 2023. Scaffolds for drug delivery and tissue engineering: the role of genetics. J. Control. Release 359, 207–223.